

# The role of triple evolution in the formation of LISA double white dwarfs

Abinaya Swaruba Rajamuthukumar<sup>1</sup>, Valeriya Korol<sup>1</sup>, Jakob Stegmann<sup>1</sup>, Holly Preece<sup>2</sup>, Rüdiger Pakmor<sup>1</sup>,  
Stephen Justham<sup>1</sup>, Silvia Toonen<sup>3</sup>, and Selma E. de Mink<sup>1,4</sup>

<sup>1</sup> Max-Planck-Institut für Astrophysik, Karl-Schwarzschild-Straße 1, 85748 Garching bei München, Germany  
e-mail: abinaya@mpa-garching.mpg.de

<sup>2</sup> Radboud Univeristy, Nijmegen

<sup>3</sup> Anton Pannekoek Institute for Astronomy, University of Amsterdam, Science Park 904, 1098, XH, Amsterdam, The Netherlands

<sup>4</sup> Ludwig-Maximilians-Universität München, Geschwister-Scholl-Platz 1, 80539 München, Germany

February 14, 2025

## ABSTRACT

Galactic double white dwarfs will be prominent gravitational-wave sources for the Laser Interferometer Space Antenna (LISA). While previous studies have primarily focused on formation scenarios in which binaries form and evolve in isolation, we present the first detailed study of the role of triple stellar evolution in forming the population of LISA double white dwarfs. In this work, we present the first detailed study of the role of triple stellar evolution in forming the population of LISA double white dwarfs. We use the multiple stellar evolution code (MSE) to model the stellar evolution, binary interactions, and the dynamics of triple star systems then use a Milky Way-like galaxy from the TNG50 simulations to construct a representative sample of LISA double white dwarfs. In our simulations about  $7 \times 10^6$  Galactic double white dwarfs in the LISA frequency bandwidth originate from triple systems, whereas  $\sim 4 \times 10^6$  form from isolated binary stars. The properties of double white dwarfs formed in triples closely resemble those formed from isolated binaries, but we also find a small number of systems  $\sim \mathcal{O}(10)$  that reach extreme eccentricities ( $> 0.9$ ), a feature unique to the dynamical formation channels. Our population produces  $\approx 10^4$  individually resolved double white dwarfs (from triple and binary channels) and an unresolved stochastic foreground below the level of the LISA instrumental noise. About 57% of double white dwarfs from triple systems retain a bound third star when entering the LISA frequency bandwidth. However, we expect the tertiary stars to be too distant to have a detectable imprint in the gravitational-wave signal of the inner binary.

**Key words.** Galaxy: stellar content – binaries (including multiple): close – white dwarfs – gravitational waves

## 1. Introduction

Observations indicate that triple star systems are common across various stellar evolutionary stages, including main-sequence stars, evolved giant stars, brown dwarfs, and black holes (Kervella et al. 2017; Faherty et al. 2011; Triaud et al. 2020; Lillo-Box et al. 2021; Rivinius et al. 2020). In particular, white dwarfs have been found in triple systems with main-sequence (MS) stars (for a review within 20 pc, see Toonen et al. 2014), other white dwarfs (Maxted et al. 2000; Perpinyà-Vallès et al. 2019), neutron stars (NSs) (Ransom et al. 2014), and brown dwarfs (BDs) (Rebassa-Mansergas et al. 2022). However, the observed number of white dwarfs in triple systems remains significantly lower than theoretical predictions, possibly due to observational biases. Indeed, Shariat et al. (2024) propose that many observed local double white dwarfs could have originated from triples. For example, a recent spectroscopic study of double white dwarfs by Heintz et al. (2024) reveals that the more massive white dwarf companion has a shorter cooling age compared to the less massive one, which contradicts the initial-final mass relation and the assumption that both stars in the binary formed simultaneously from the same molecular cloud. One proposed explanation is that the progenitors of the double white dwarf were originally in a triple system, where the massive white dwarf was formed by the merger of two stars, resulting in a shorter cooling age. Furthermore, triples could significantly contribute

to the rate of Type Ia supernovae, making a substantial contribution to that from isolated binary stars (Katz et al. 2011; Hamers et al. 2013; Rajamuthukumar et al. 2023).

Hierarchical triple systems are characterized by a close inner orbit and with a tertiary component in a wider orbit. When the orbits of the inner and outer stars are sufficiently inclined, the gravitational perturbation from the tertiary star can cause large-amplitude von Zeipel-Lidov-Kozai (ZLK) oscillations (von Zeipel 1909; Lidov 1962; Kozai 1962) oscillations of the inner binary eccentricity whilst the semi-major axis is unchanged. This process can play a key role in the formation of close binaries. The combination of ZLK oscillations with dissipative effects like tidal friction (Kiseleva et al. 1998; Eggleton & Kiseleva-Eggleton 2001; Fabrycky & Tremaine 2007) and gravitational-wave radiation can lead to a reduction in the inner binary's orbital semi-major axis. Thus, perturbations from the tertiary star can facilitate close-binary processes such as mass transfer, common-envelope phases, mergers, and collisions in the inner binary (Fabrycky & Tremaine 2007; Perets & Kratter 2012; Shappee & Thompson 2013; Hamers et al. 2013; Michaely & Perets 2014; Antonini et al. 2017; Toonen et al. 2020; Hamers & Thompson 2019; Stegmann et al. 2022a,b).

Gravitational-waves from compact double white dwarfs (with frequencies ranging from  $10^{-4}$  to  $10^{-1}$  Hz) detectable with the upcoming Laser Interferometer Space Antenna (LISA) mission offer a unique way to explore these triple systems (Amaro-

Seoane et al. 2023). By detecting the gravitational-wave signals from double white dwarfs, LISA could uncover a population of systems formed through the triple evolution channel which are inaccessible to electromagnetic observations. This capability has the potential to provide new insights into the formation mechanisms of double white dwarfs, their contribution to Type Ia supernovae (Iben & Tutukov 1984), and the broader implications for the chemical evolution of the Galaxy (Pagel 1997).

LISA is expected to detect  $\sim O(10^6)$  of Galactic double white dwarfs as part of an unresolved confusion gravitational-wave background and individually resolve around  $10^3 - 10^4$  of the 'loudest' double white dwarfs (e.g., Korol et al. 2017; Lamberts et al. 2019; Thiele et al. 2023; Wilhelm et al. 2021; Li et al. 2023; Tang et al. 2024). While these previous studies have focussed on double white dwarfs formed from the evolution of isolated binary stars, increasing evidence suggests that hierarchical triple systems, in which a close inner binary is orbited by a distant tertiary companion, may also play a significant role in the formation of double white dwarfs (Toonen et al. 2020; Heintz et al. 2024; Shariat et al. 2024).

There is mounting observational evidence that stars often form with bound companions, with a binary fraction of 30% and a triple fraction of 10% for F and G-type stars (i.e. with masses  $\sim 1 M_{\odot}$ ) (Eggleton & Tokovinin 2008; Raghavan et al. 2010; Tokovinin 2014; Moe & Di Stefano 2017; Offner et al. 2023). Moreover, the inner binaries in triple systems tend to be in closer orbits than the binaries found in isolated systems, which increases the probability for some binary interactions (Toonen et al. 2020). In this paper, we show that triple systems offer a greater number of evolutionary pathways for forming short-period inner binaries compared to isolated binary systems.

Previous studies have explored the potential for detecting tertiary companions in LISA data (e.g., Seto 2008; Robson et al. 2018; Tamanini & Danielski 2019). Similar to electromagnetic observations, the motion of the double white dwarf around the center of mass of the triple system modulates the gravitational-wave frequency through the Doppler effect. This modulation causes a periodic shift in the gravitational-wave frequency, oscillating around the intrinsic frequency of the inner binary. Recent studies have focused on leveraging this effect to detect sub-stellar mass tertiaries, such as exoplanets and brown dwarfs (Tamanini & Danielski 2019; Danielski et al. 2019; Kang et al. 2021; Katz et al. 2022). Thus, previous studies have primarily focused on either the isolated binary population of double white dwarfs or the detection possibilities of the third star. Our work is the first evolutionary population synthesis study of Galactic double white dwarfs resulting from triple evolution. In addition, our study accesses the impact of the triple evolution channel to the LISA's astrophysical noise background, thereby influencing the  $\rho$  of all other gravitational-wave sources.

We aim to quantify the contribution of the triples to the population of double white dwarfs detectable by LISA. We combine population synthesis models using the Multiple Star Evolution (MSE) code (Hamers et al. 2021) with cosmological simulations from the TNG50 project (Nelson et al. 2019; Pillepich et al. 2019) to construct a representative model of the Galactic double white dwarf population. Our study addresses two critical questions: 1) What fraction of double white dwarfs detectable by LISA originates from the triple evolution channel? 2) Can LISA detect the dynamical effects of the third star in these triple systems?

The paper is structured as follows. In Section 2, we explain our methodology. Section 3 describes the evolutionary pathways of triples that lead to the formation of LISA double white dwarfs. We detail the population properties of LISA double white dwarfs

from isolated binaries and triples in Section 4, investigating prospects for direct detection of the third star in Section 4.4. Finally, we discuss the results in Section 5 and summarise our findings in Section 6.

## 2. Methods

All simulations are performed using the publicly available population synthesis code MSE<sup>1</sup> (Hamers et al. 2021). Our set of simulations of hierarchical triples consists of a main run with a choice of default parameters and three model-variant runs. In each simulated data set, we evolve the triples from the start of the zero-age-main-sequence until a maximum integration time  $t_{\max} = 14$  Gyr. The main triple data set consists of  $10^5$  systems, where we adopt a common envelope efficiency parameter  $\alpha_{\text{CE}} = 1$ , and all three stars are assumed to have formed at solar metallicity  $Z = Z_{\odot} = 0.02$ . This population results in  $3 \times 10^3$  LISA double white dwarfs, yielding a  $\sim 2\%$  Poisson error. In each of the three model-variant runs, we simulate  $10^4$  systems and either vary the common envelope efficiency parameter as  $\alpha_{\text{CE}} = 0.1$  and 10 or change the metallicity of the stars to sub-solar  $Z = 0.1 Z_{\odot}$ . The effects of the chosen parameters are discussed in Section 5. In addition to the triple runs, we simulate a population of  $10^5$  isolated binaries to compare the impact of tertiary companions. Additionally, we model the inner binaries of all triples without their tertiary stars to assess their influence on the resulting LISA double white dwarf population. We expect that the isolated binary population differs significantly from the inner binary population of triples. The primary distinction is that the inner binaries have much more compact semi-major axes due to the dynamical stability constraints imposed by the tertiary star.

This section details the physics of the single, binary, and triple evolution incorporated into MSE, and outlines our initial distributions for the stellar populations. Additionally, we provide an overview of the Milky Way-like galaxy selected from the cosmological simulation TNG50. This Milky Way-like galaxy is then used to seed double white dwarfs in the galaxy. The methodology for constructing the Galactic double white dwarf population from triples is also explained here, while further details on building the Galactic double white dwarf population from isolated binaries are provided in the appendix.

### 2.1. Multiple stellar evolution code (MSE)

We use the population synthesis approach using the code MSE to model the stellar evolution, binary interactions (tides, mass transfer, etc.), dynamical perturbations from higher-order companions in multiple systems, and fly-bys from ambient stars. MSE is a C/C++ code with a Python interface that can handle any number of stars as long as they start in a hierarchical arrangement. MSE uses a hybrid approach that switches between the secular approximation for dynamically stable orbits (that satisfy the criterion of Mardling & Aarseth 2001) and direct  $N$ -body integration using MSTAR (Rantala et al. 2020) for dynamically unstable orbits. Throughout the evolution post-Newtonian terms are included to 2.5 order in the secular approximation and to 3.5 order for the direct  $N$ -body integration.

To follow the evolution of single stars, MSE relies on the fitting formulae from Hurley et al. (2000); Tout et al. (1996), while binary interactions such as tides, wind mass transfer, stable mass transfer episodes, and common envelope (CE) evolutions are

<sup>1</sup> <https://github.com/hpreece/mse>.

computed using modified prescriptions of Hurley et al. (2002). We briefly explain the physical handling of these key processes below. For more detailed explanations see Hamers et al. (2021).

*Stable mass transfer:* In MSE, mass transfer stability is determined either by the critical mass ratio criterion or by comparing mass transfer and dynamical timescales. The critical mass ratio depends on the donor’s stellar type (Hamers et al. 2021). We assume fully conservative mass transfer ( $\beta_{\text{MT}} = 1$ ), meaning no mass is lost from the system. While MSE generally follows Hurley et al. (2002) for binary interactions, it differs in treating mass transfer in eccentric orbits. Hurley et al. (2002) assumes tides are always efficient in circularizing the orbit. However, in triple systems, the eccentricities are excited secularly. We follow the analytical model from Hamers & Dosopoulou (2019) to model mass transfer at periastron in eccentric orbits.

*Common envelope evolution:* Unstable mass transfer/CE evolution in MSE follows the  $\alpha_{\text{CE}}$  prescription (Paczynski 1976; van den Heuvel 1976; Livio & Soker 1988; Iben & Livio 1993; Hurley et al. 2002). The code solves for orbital energies before and after the CE phase, parameterizing the envelope ejection efficiency by  $\alpha_{\text{CE}}$  and assuming a binding energy factor of  $\lambda = 1$ . For the main runs, we adopt  $\alpha_{\text{CE}} = 1$  and common envelope time of  $10^3$  yr. The post-CE semi-major axis is determined from the corresponding orbital energy.

*Merger/collision:* A “failed” CE can result in the merger of two stars. This occurs if the post-CE semi-major axis is too small for either star to avoid Roche lobe overflow. Beyond post-CE mergers, MSE also accounts for physical collisions when the sum of the stellar radii exceeds the semi-major axis or when a periastron collision occurs in an eccentric orbit. The properties of the merger remnant are assigned following Hurley et al. (2002).

*Contact evolution:* If both stars simultaneously fill their Roche lobes, MSE assumes a CE phase if both are giant stars. Otherwise, a merger is assumed.

*Triple common envelope (TCE) evolution:* Mass transfer from a third star onto the inner binary can lead to a TCE. If CE conditions are met for the third star, MSE employs “circumstellar triple CE evolution”, allowing the third star to fill its Roche lobe around the inner binary and undergo unstable mass transfer. This follows a similar approach to the prescription proposed by Comerford & Izzard (2020). The final outer semi-major axis is estimated using an  $\alpha_{\text{CE}}$  prescription, assuming the inner binary remains relatively compact. However, CE modeling is inherently uncertain (see Ivanova et al. 2013 for a review), and TCE evolution is even more so, requiring cautious interpretation of results. For detailed hydrodynamical simulations of triple CE outcomes, see e.g. Glanz & Perets (2020).

*fly-bys:* MSE also includes the gravitational perturbations from stellar fly-bys in the vicinity of the system using the impulsive approximation. The fly-by mass is sampled from a Kroupa initial mass function (Kroupa 2001), and encounters are randomly sampled within an encounter sphere of radius  $R_{\text{enc}} = 10^5$  au with velocities drawn from a Maxwellian velocity distribution with dispersion  $\sigma_{\star} = 30$  km s $^{-1}$ . The number density of fly-bys accounts for the low-density environments, assuming  $n_{\star} = 0.1$  pc $^{-3}$ . These fly-bys become significant for the evolution of the system if the semi-major axis of the outer orbit exceeds about  $10^3$  au (Jiang & Tremaine 2010; Grishin & Perets 2022; Stegmann et al. 2024).

## 2.2. Initial conditions

Here, we describe the initial distribution of our synthetic population of stars. We denote the masses of the inner binary compo-

nents as  $m_1$  and  $m_2$ , where  $m_1 \geq m_2$ , and the mass of the tertiary companion as  $m_3$ . Semi-major axes are denoted as  $a_1$  for the inner binary and  $a_2$  for the outer binary. Orbital eccentricities are denoted as  $e_1$  and  $e_2$ , respectively. Figure 1 shows the distribution of the parameters of the initial triple population.

We draw the primary mass  $m_1$  from a Kroupa initial mass function (Kroupa 2001) between 1 and  $8 M_{\odot}$ . Furthermore, we follow functions from Moe & Di Stefano 2017 to sample the orbital period ( $0.2 \leq \log(T_1/\text{days}) \leq 8$ ) and secondary mass ( $0.08 M_{\odot} \leq m_2 \leq m_1$ ) of the inner binary, and calculate the semi-major axis  $a_1$  from Kepler’s law. Similarly, the orbital period of the outer binary also follows Moe & Di Stefano 2017, where we assume that the inner binary is represented as a single star with a mass of  $m_1 + m_2$ . We allow the tertiary mass  $m_3$  to be more massive than the total mass of the inner binary in certain cases and an extrapolated mass ratio distribution from Moe & Di Stefano 2017 is used to sample  $m_3$ . In addition, we sample the eccentricities of inner ( $e_1$ ) and outer ( $e_2$ ) orbit from Moe & Di Stefano 2017 and randomly sample the spatial orientations of the inner and outer orbital frames from isotropic distributions.

We reject any star whose radius exceeds the Roche lobe radius on the zero-age main sequence (Eggleton 1983) and reject any system which would be dynamically unstable (Vynatheya et al. 2022) at the start of the simulation. Any Roche lobe overflow or dynamical instabilities are modeled using prescriptions in MSE during the evolution (see Section 2.1 for more details).

## 2.3. Construction of Galactic double white dwarf population

We use a Milky Way-like galaxy from the large-scale cosmological magneto-hydrodynamical simulations TNG50 (Nelson et al. 2019; Pillepich et al. 2019). With a comoving volume of  $(50 \text{ Mpc})^3$  the TNG50 simulation box contains about 100 Milky Way-like galaxies with a total mass of  $10^{14} M_{\odot}$ . To select a suitable Milky Way-like galaxy, we randomly choose one of the six halos with a total mass  $1 - 2 \times 10^{12} M_{\odot}$  and whose central galaxy has a stellar mass  $5 - 7 \times 10^{10} M_{\odot}$ . Additionally, we examine the galaxy’s stellar projection to confirm disk dominance. The mass of the selected galaxy (Galaxy ID = 476266) is  $\sim 5 \times 10^{10} M_{\odot}$  which is consistent with our Milky way galaxy (e.g. Bland-Hawthorn & Gerhard 2016). We extract present-day properties such as age, stellar mass, and 3D-position of the star particles. We place our observer at a randomly assigned Sun-like position in the disk, 8.2 kpc from the Galactic center. We then measure the distances to all LISA-detectable double white dwarfs from each star particle to this location. We combine these Galactic properties with the simulated triples to construct a representative Galactic double white dwarf population as follows.

From the  $10^5$  simulated triples with MSE, we select those which form double white dwarfs that emit gravitational waves in the LISA frequency bandwidth ( $10^{-4}$  Hz – 0.1 Hz) during their evolution. We use this sample to assemble the entire Galactic LISA double white dwarf population in each star particle of the selected TNG50 Milky Way-like galaxy. In our simulated sample all the stars are assumed to be formed simultaneously. To allow for continuous star formation we seed the number of LISA double white dwarfs per star particle ( $N_{\text{DWD},\star}$ ) based on the age and stellar mass ( $M_{\star}$ ) of the star particle as:

$$N_{\text{DWD},\star} = \frac{N_{\text{DWD,MSE}}}{M_{\text{tot,MSE}}} \times M_{\star}, \quad (1)$$

where  $N_{\text{DWD,MSE}}$  is the total number of all double white dwarfs in MSE which emit gravitational waves in the frequency bandwidth of LISA at a simulation time equal to the age of the star

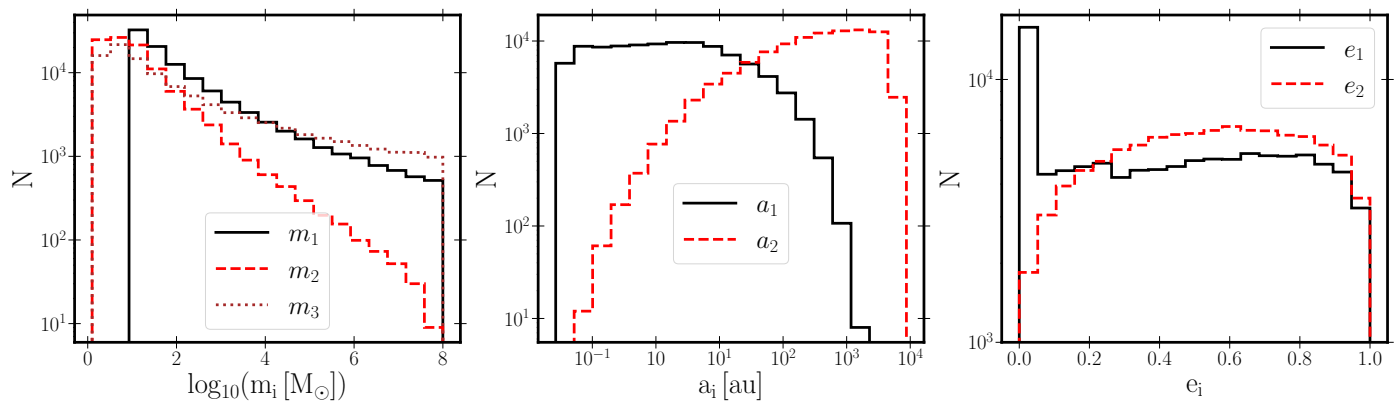


**Fig. 1.** Initial parameter distributions. The left panel shows the mass distributions, where  $m_1$  and  $m_2$  denote the masses of the inner binary components, and  $m_3$  represents the mass of the tertiary. The middle panel displays the semi-major axis distributions for the inner ( $a_1$ ) and outer ( $a_2$ ) orbits, respectively. The right panel illustrates the eccentricity distributions of the inner ( $e_1$ ) and outer ( $e_2$ ) orbits, respectively. See Section 2.2 for more details.

particle and  $M_{\text{tot, star particle}}$  is the mass of the star particle at  $z = 0$ , which is obtained from the TNG50 simulation. The total stellar mass of the simulated population is given by

$$M_{\text{tot, MSE}} = \frac{N_{t, \text{in range}}}{f_{t, \text{in range}} \cdot f_t} \cdot [f_t \cdot \bar{m}_t + f_b \cdot \bar{m}_b + (1 - f_t - f_b) \cdot \bar{m}_s],$$

for  $f_t \neq 0$ ,

(2)

where  $N_{t, \text{in range}} = 10^5$  is the number of simulated triple systems with MSE,  $f_{t, \text{in range}}$  is the fraction of triples in this range relative to a wider mass range of stars ( $0.08 M_\odot - 100 M_\odot$ ), and the triple fraction  $f_t = 0.2$ , binary fraction  $f_b = 0.3$ , and single star fraction  $1 - f_t - f_b = 0.5$  represent the fractions of triple, binary, and single systems in a full stellar population (Moe & Di Stefano 2017). We assumed a more optimistic triple fraction than currently estimated from observations to account for the incompleteness. However, our results can be rescaled for practically any assumed triple fraction. The parameters  $\bar{m}_t = 3.5 M_\odot$ ,  $\bar{m}_b = 0.9 M_\odot$ , and  $\bar{m}_s = 0.5 M_\odot$  denote the numerically computed average masses of triple, binary, and single systems, respectively. The first term of Eq. (1) represents the total contribution to the stellar mass from triple systems, scaled by their fraction in the population and their average mass. The second term accounts for the contribution from binary systems and the third term represents the mass contribution from single stars. The multiplicative term  $N_{t, \text{in range}} / (f_{t, \text{in range}} \cdot f_t)$  re-scales the number of simulated triples in the simulated mass range ( $1 - 8 M_\odot$ ) to the total number of stellar systems in the full mass range ( $0.08 - 100 M_\odot$ ), accounting for the fraction of triples in the full population ( $f_t$ ) and their relative contribution to the restricted range ( $f_{t, \text{in range}}$ ).

Using Eq. (1), we seed the number  $N_{\text{DWD}, \star}$  of LISA-detectable double white dwarfs corresponding to each star particle and randomly select them from our simulated sample (for  $N_{\text{DWD}, \star} > N_{\text{DWD}, \text{MSE}}$  a star particle contains some sampled double white dwarfs more than once). Additionally, we assume that all double white dwarfs are located at a star particle's center of mass.

### 3. Key processes that shape the triple evolutionary pathways

In this section, we present a brief overview of the five key processes characteristic of triple evolution that shape the evolutionary pathways leading to the formation of LISA double white dwarfs:

1. *Induced mass transfer:* The perturbation from the tertiary star triggers mass transfer in the inner binary, altering its timing or evolutionary phase compared to an isolated binary. This process ultimately leads to the formation of a short-period LISA double white dwarf.
2. *Outer binary channel:* The inner binary stars merge and form a new rejuvenated star which then evolves with the tertiary star to become a LISA double white dwarf.
3. *Ejected tertiary:* The tertiary star aids the formation of the inner double white dwarf but becomes unbound before it enters the LISA frequency bandwidth.
4. *Triple common envelope:* The third star initiates mass transfer onto the inner binary, leading to the formation of a LISA double white dwarf.
5. *Inner binary channel:* The tertiary companion remains bound to the inner binary throughout its evolution but is too distant to significantly affect the formation of a double white dwarf; this channel is effectively that of the isolated binary channel.

We show a schematic diagram for primary processes that drive evolutionary pathways leading to LISA double white dwarfs from triples in Figure 2. In the following subsections, we discuss these processes in greater depth with detailed examples. All error bars presented below are estimated by scaling up the fractional Poisson error from the intrinsic population evolved with MSE. Figure 3 shows that the processes are not mutually exclusive. For instance, about 4.8% of Galactic LISA double white dwarfs from triples undergo a TCE phase and induced mass transfer, leading to a merger in the inner binary. Hence, the relative percentages quoted below do not add up to 100%.

#### 3.1. Induced mass transfer

When comparing the triple runs to the inner binary runs (where the inner binary from the same triple population evolves without the tertiary star; see Section 2). We find that approximately

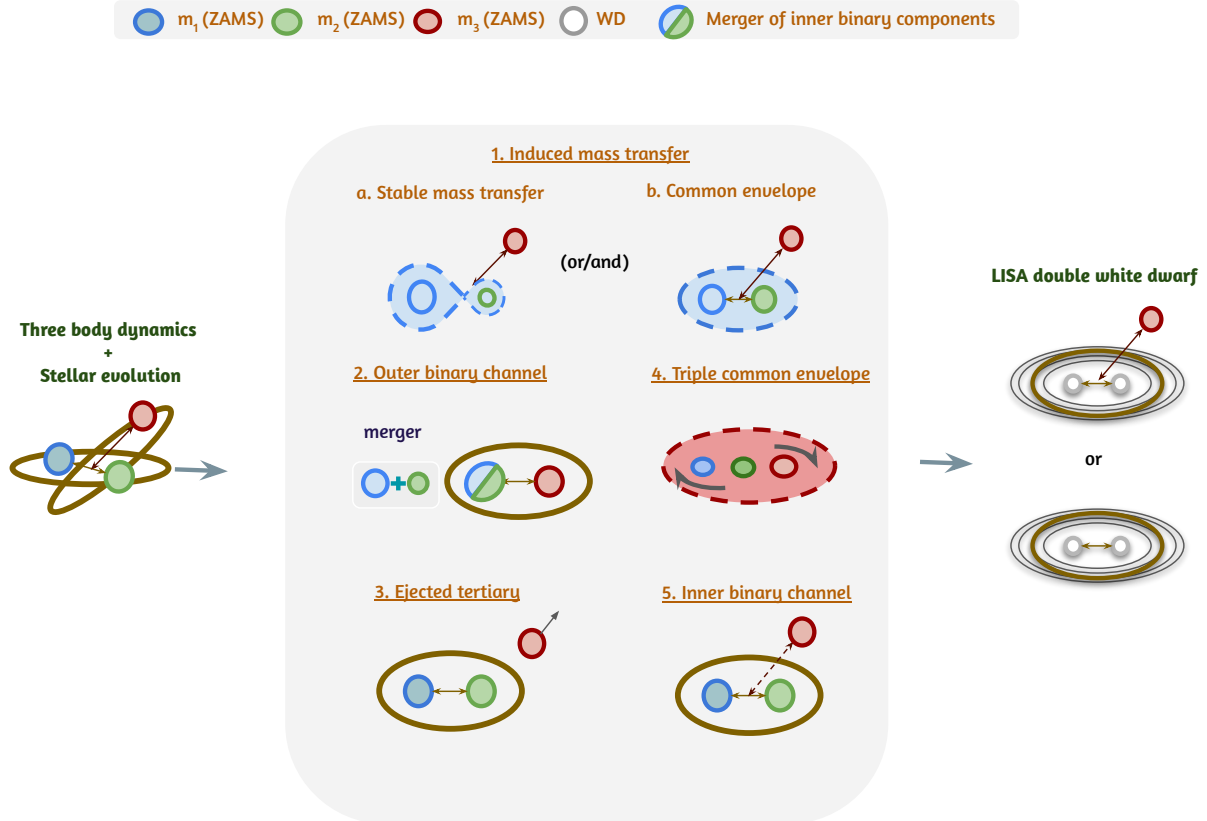


**Fig. 2.** A schematic diagram of possible key processes that drive the evolutionary phases of a triple evolution leading to the formation of a double white dwarf in the LISA frequency bandwidth. The diagram showcases key stages, including mass transfer, common envelope phases, ZLK oscillations that enhance eccentricity, and eventual binary evolution. The tertiary star plays a critical role in shaping the inner binary’s dynamics, either by inducing orbital changes or facilitating interactions that lead to the formation of the LISA double white dwarf. Blue and green circles represent the inner binary main-sequence stars. A red circle with an arrow pointing to the inner binary represents the tertiary star. A dashed arrow indicates a distant tertiary star that is too far to significantly influence the inner binary. Circles inside a brown solid ellipse show the binary. A dashed circle represents the common envelope process. A white circle represents a white dwarf, and a multi-colored circle represents a post-merger star.

$9.0\% \pm 0.1\%$  of the Galactic LISA double white dwarfs undergo a mass transfer episode solely induced by the presence of a third star. These inner binaries would not have interacted over a Hubble time without the presence of the tertiary star. About  $52\% \pm 10\%$  of Galactic LISA double white dwarfs initiate mass transfer at a different time due to the influence of a tertiary star. Thus, a total of 61% of systems experience induced mass transfer (see Figure 3). In contrast, the corresponding isolated binaries would either not undergo mass transfer or interact at a different time. This timing difference for the onset of mass transfer is crucial for driving the merger in the inner binary or forming a short-period inner binary that can enter the LISA frequency bandwidth within Hubble time (see the below example for more details). Also, we note that only a negligible fraction ( $\sim 10^{-6}$ ) of systems undergo stable mass transfer without eventually becoming unstable.

As examples we show the evolution of a triple system and the inner binary without the tertiary star in Figure 4. The triple system starts with  $m_1 = 1.61 M_\odot$ ,  $m_2 = 1.28 M_\odot$ , and  $m_3 = 1.16 M_\odot$  as the tertiary star. The inner binary is initially eccentric, with an eccentricity  $e_1 = 0.18$  and a semi-major axis  $a_1 = 42.6$  au, while the tertiary orbit is much wider, with a semi-major axis of

$a_2 \approx 2980$  au and an eccentricity of  $e_2 = 0.26$ . The initial mutual inclination between the inner and outer orbits is  $99^\circ$ . Without the tertiary star the system evolves as an isolated binary. The relatively large initial semi-major axis allows the binary components to evolve into white dwarfs without a mass transfer episode. During the course of evolution of the binary mass loss due to winds further widens the system, as shown in Figure 5. The system continues to lose orbital energy via gravitational-wave radiation but remains too wide ( $a \approx 32.1$  au) to enter the LISA frequency bandwidth within a Hubble time. However, with the third star present, the system undergoes significant orbital shrinkage of the inner binary during its evolution and ultimately enters the LISA frequency band. At around 2.2 Gyr, the primary star of the inner binary becomes a red giant with a convective envelope. The ZLK effect, combined with tidal friction (Fabrycky & Tremaine 2007), shrinks the inner binary’s orbit from  $a_1 \approx 42.6$  au to 1 au. This shortening allows the primary star to fill its Roche lobe and initiate mass transfer to its companion. The mass transfer becomes unstable due to the high mass ratio and the system enters a CE phase, which further reduces the inner binary’s orbit to 0.1 au. This results in a  $0.41 M_\odot$  white dwarf and a  $1.28 M_\odot$  main-sequence star. Later, at around 5 Gyr, the main-sequence

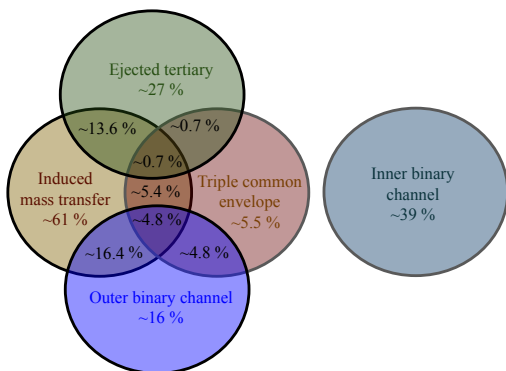


**Fig. 3.** A Venn diagram illustrating the overlap of the different evolutionary processes. Among the five processes, the Inner Binary channel is the only one that does not require mandatory assistance from the tertiary star to produce a LISA double white dwarf. In contrast, the other four processes rely on the tertiary star to bring the system into the LISA frequency bandwidth. These processes are not mutually exclusive and exhibit significant overlap.

companion evolves to an AGB star, eventually leading to a second CE phase. This produces a short-period double white dwarf with component masses of  $0.41 M_{\odot}$  and  $0.23 M_{\odot}$ , which enters the LISA frequency bandwidth after a few million years. Thus, in this example, the binary would not be to become a LISA source without the tertiary.

### 3.2. Outer binary channel

About  $16.0\% \pm 0.3\%$  of Galactic LISA double white dwarfs originate from triples where there was a merger of the inner binary stars. We identify four scenarios which lead to mergers. First, if the inner and outer orbital planes are highly inclined with respect to each other, the perturbations from the tertiary companion shrinks the orbit of the inner binary through the combination of the ZKL effect and tides. The tightened triple system has an earlier CE episode than in an isolated binary. The CE evolution results in a merger, forming a rejuvenated star bound to the former tertiary star as a binary system. This binary can evolve into the LISA frequency bandwidth. Second, in comparison to the first, the triples start out with a relatively short-period inner binary and a distant tertiary. Here, the binary comes into contact and merges without the aid of the tertiary star. The merged star further evolves with the tertiary star to enter the LISA frequency bandwidth. Third, a TCE can cause a merger of the inner binary stars (see Section 3.4 for more details). Fourth, the orbit of the inner binary can widen due to mass transfer and winds, making the entire system dynamically unstable which eventually leads a chaotic evolution of the orbits and the merger of the inner binary stars.

Panel (a) of Figure 6 shows an example where the inner binary merges to form a new star. The system starts with  $m_1 = 3 M_{\odot}$  and  $m_2 = 2.94 M_{\odot}$ , and  $m_3 = 1.89 M_{\odot}$  as the tertiary star. The inner binary is initially circular with a semi-major axis  $a_1 = 0.3$  au. The tertiary orbit is relatively tight, with an outer semi-major axis  $a_2 = 4.7$  au and is eccentric with  $e_2 = 0.56$ . The mutual inclination between the inner and outer orbits is  $62^{\circ}$ . The most massive of all three stars is in the inner binary ( $m_1 = 3 M_{\odot}$ ) which, at about 370 Myr, initiates an unstable mass transfer episode onto the secondary resulting in the merger of the two stars. This merger leads to the formation of a new star with a mass  $m_r = 5.69 M_{\odot}$ . The remaining post-merger binary com-

posed of the rejuvenated star and the tertiary companion subsequently undergoes and survives two more CE episodes: one when the rejuvenated star enters the AGB at about 390 Myr and another when the tertiary companion becomes a red giant star at about 1.4 Gyr. The second CE leads to the formation of a circular double white dwarf with a semi-major axis of  $9 \times 10^{-3}$  au later entering the LISA bandwidth after  $\sim 1$  Gyr. An isolated binary with the same properties as the inner binary of such triple would not enter the LISA band.

### 3.3. Ejected tertiary

About  $27.0\% \pm 0.4\%$  of Galactic double white dwarfs from triples lost the tertiary star. The unbinding of the tertiary companion primarily occurs due to the following reasons. First, during a CE phase the inner binary's orbit shrinks and loses angular momentum, while the prompt mass loss during the CE unbinds the outer orbit. Second, if the inner binary widens due to mass transfer or stellar winds the system becomes less hierarchical and dynamically unstable. Dynamically unstable orbits lead to chaotic evolution which may eject an object from the system. We provide a specific example of this process below.

Panel (b) of Figure 6 shows an example of a system where a tertiary gets ejected after a CE in the inner binary. The system starts with  $m_1 = 1.39 M_{\odot}$  and  $m_2 = 1.39 M_{\odot}$  as the inner binary components and  $m_3 = 0.31 M_{\odot}$  as the tertiary star. The inner binary is initially eccentric with an inner eccentricity  $e_1 = 0.56$  and an inner semi-major axis  $a_1 = 50.1$  au. The tertiary orbit is wide, with an outer semi-major axis  $a_2 \approx 1690$  au and is eccentric with  $e_2 = 0.81$ . The mutual inclination between the inner and outer orbits is  $112^{\circ}$ . The inner binary masses are greater than the tertiary star so they evolve on a shorter timescale. The CE occurs in the inner binary during the AGB phase after about 3.6 Gyr. The CE reduces the inner binary semi-major axis to  $10^{-2}$  au and unbinds the outer tertiary. The remaining binary components evolve into a double white dwarf system. This double white dwarf binary emits gravitational-waves and later enters the LISA frequency bandwidth after 1 Myr. In this example, even though the binary does not have a bound tertiary star by the time it enters the LISA frequency bandwidth, the tertiary plays a role in shrinking the binary before the CE episode.

### 3.4. Triple common envelope

About  $5.5\% \pm 0.1\%$  of Galactic double white dwarfs from triples undergo a phase of TCE evolution before entering the LISA frequency band. We identify two possible evolutionary outcomes of a TCE event in our simulations. First, the merger of the inner binary: the inner binary may merge to form a rejuvenated star. The new star forms a binary with the third star which later enters LISA frequency bandwidth. Second, ejection of one component: One of the stars may become unbound from the system, leaving behind a binary formed by the remaining two stars. This binary may enter the LISA band. We explain one of the examples below (see Hamers et al. 2022 for a more detailed study of TCE).

Figure 7 shows an example of a TCE where the inner binary merges to form a new binary. The system starts with  $m_1 = 1.18 M_{\odot}$ ,  $m_2 = 0.54 M_{\odot}$ , and a relatively massive tertiary  $m_3 = 5.59 M_{\odot}$ . The inner binary is initially circular, with a semi-major axis  $a_1 = 0.05$  au. The tertiary orbit is compact, with an outer semi-major axis  $a_2 = 25$  au and highly eccentric with  $e_2 = 0.94$ . The mutual inclination between the inner and

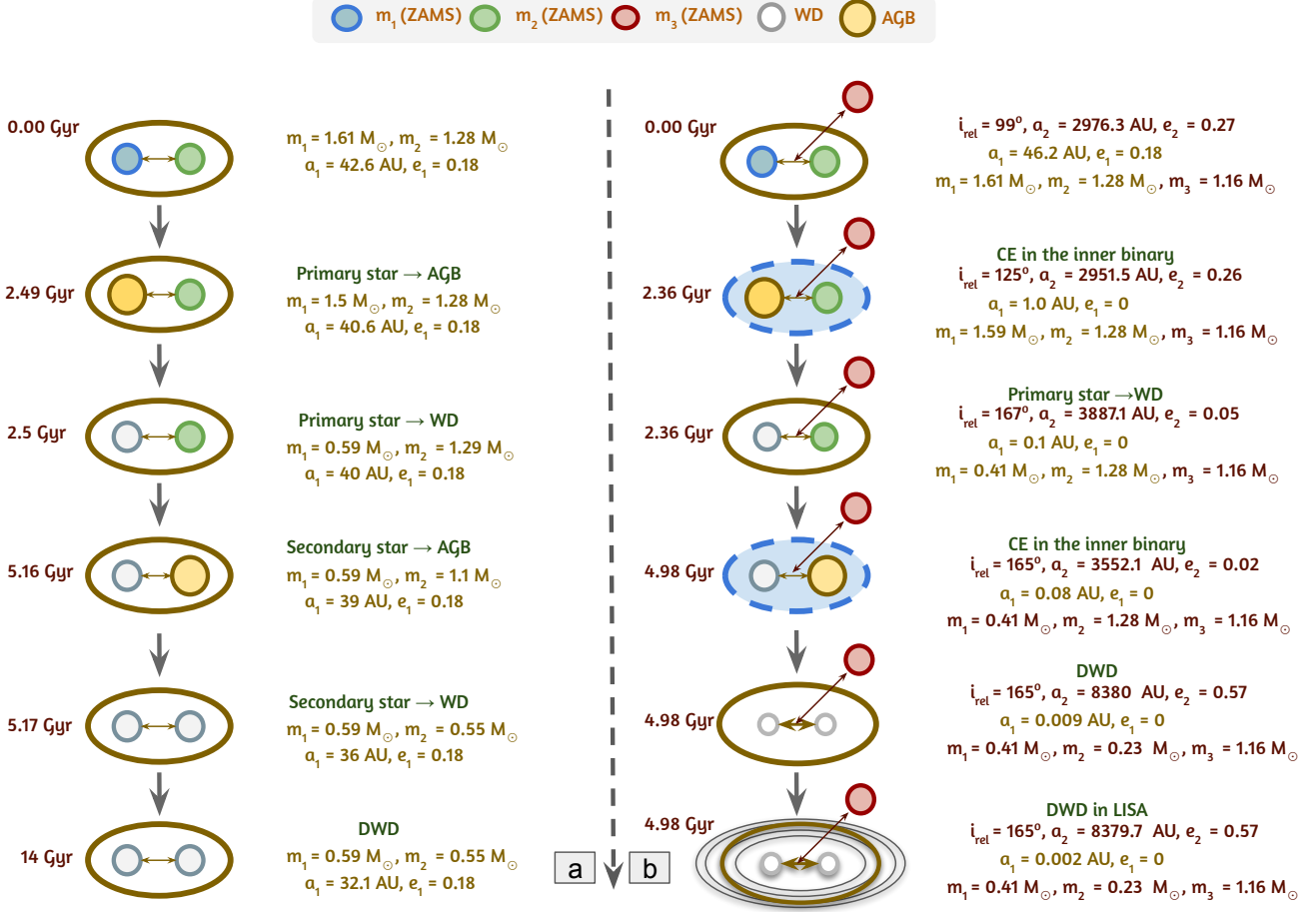


**Fig. 4.** Comparison of the evolution of a triple system with and without a tertiary star. Panels (a) and (b) illustrate the evolution of the inner binary with and without the third star respectively. In the system with the tertiary star, mass transfer is induced by perturbations from the third star, allowing the system to eventually enter the LISA frequency bandwidth. When evolved without a tertiary star the binary components remain too far apart to interact. Such a system does not enter the LISA frequency bandwidth. The legends are similar to those in Figure 2. In addition, the yellow circle represents a star in the AGB phase.

outer orbit is  $160^\circ$ . Since the tertiary star is massive compared to the inner binary masses, it is the first to reach the AGB phase, in about 92 Myr. The inner binary components are still on the main-sequence.

Expansion of the envelope during the AGB phase initiates Roche lobe overflow. The AGB tertiary starts transferring mass onto the inner binary. The mass transfer becomes dynamically unstable owing to a higher mass ratio. The envelope of the AGB tertiary star engulfs both components of the inner binary. The TCE evolution leads to interactions between the three stars. The inner binary merges to form a rejuvenated star which is still bound to the stripped tertiary star. The resulting binary has a large eccentricity of 0.73 and a semi-major axis of 0.2 au.

After approximately 2 Gyr, the rejuvenated star evolves into a red giant which transfers mass onto the white dwarf, initiating another CE phase. The end of this CE phase leaves a circular and compact double white dwarf in a circular orbit with a semi-major axis of  $\sim 9 \times 10^{-3}$  au. After a few million years the binary enters the LISA frequency bandwidth due to gravitational-wave emission. Here, TCE plays a significant role as it leads to merging the inner binary. The binary with the post-merger rejuvenated star later enters the LISA frequency bandwidth. Hence, the tertiary star plays a vital role in the evolution of the triple to LISA frequency bandwidth.

### 3.5. Inner binary channel

The inner binary channel is similar to the isolated binary channel, where the binary evolves without a notable contribution from the tertiary star. About  $39.0\% \pm 0.7\%$  of the Galactic double white dwarfs from triples in our simulations follow this channel. Here the inner binary undergoes phases of CE before forming a short-period double white dwarf. This double white dwarf later enters the LISA frequency bandwidth with either a wide tertiary or as a binary with an ejected tertiary (for details on ejected tertiary, see Section 3.3).

## 4. LISA double white dwarfs: isolated binary vs. triple evolution

Building on the method in Section 2.3, where we construct the Galactic population by combining MSE with a Milky Way-like galaxy from TNG50, we obtain a total of  $\sim 7.2 \times 10^6$  Galactic double white dwarfs originating from triples. To compare this result with the isolated binary channel, we adjust our simulation as described in Appendix A. We emphasize that the initial distribution of the isolated binary population is constructed to represent truly isolated binaries and is different from the initial properties sampled to assemble the inner binaries in triple systems (cf. Section 2.2). In the isolated binary case, we find that

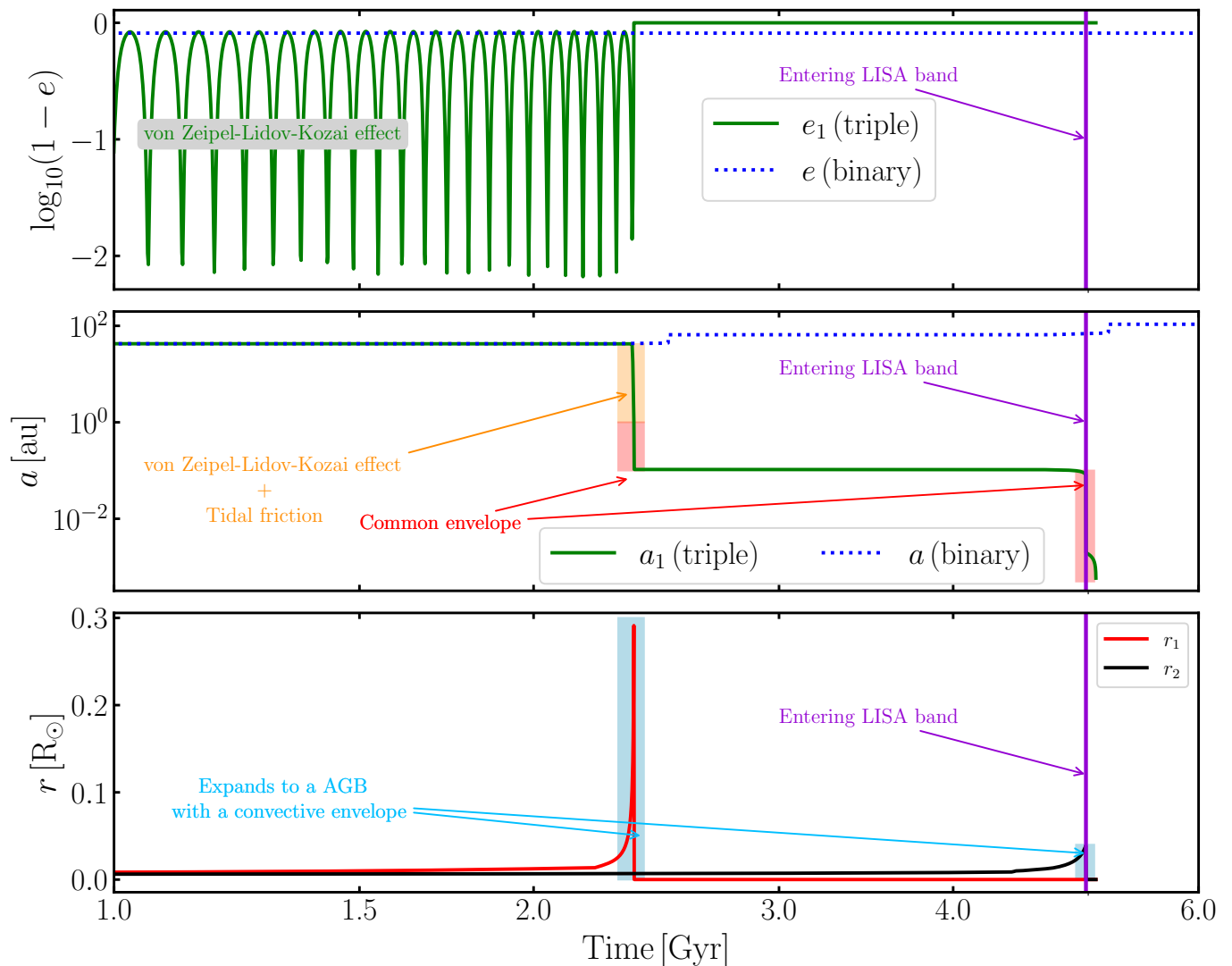


**Fig. 5.** Comparative evolution of the properties of the inner binary of the triple with and without a third star. The three panels from top to bottom display the zoomed-in evolution of key parameters: eccentricity, semi-major axis, and radius of the two stars, respectively. In the case of the triple system, the inner binary experiences unstable mass transfer, causing it to shrink further and eventually enter the LISA band. Meanwhile, the inner binary when evolved without a tertiary star undergoes mass loss due to winds, resulting in an increase in its semi-major axis and a widening of the orbit. Here  $a_1$  (triple) and  $e_1$  (triple) represent the semi-major axis and eccentricity of the inner binary evolved with a tertiary star, while  $a_1$  (binary) and  $e_1$  (binary) show the semi-major axis and eccentricity of the same inner binary evolved without the tertiary star. Additionally,  $r_1$  and  $r_2$  represent the radii of the primary and secondary stars in the inner binary, respectively.

about  $\sim 3.8 \times 10^6$  double white dwarfs are produced through isolated binary evolution, yielding a total of  $\sim 1.1 \times 10^7$  Galactic double white dwarfs emitting gravitational waves within the LISA bandwidth. Thus, approximately 65% ( $\sim 7.2 \times 10^6$ ) of all Galactic double white dwarf binaries is originated from triple systems as illustrated in Figure 8. We note that the isolated binary evolution channel only yields circular binaries. In contrast, the triple channel generates a small fraction ( $3 \times 10^{-6}$ ) of eccentric binaries, which we will discuss below.

Notably, we find that among all the double white dwarfs initially in triples only about half ( $\sim 57\%$ ) retain a bound tertiary. In the remaining systems the third star either becomes unbound or merges with another star within the system to form a binary. Importantly, all double white dwarfs that retain their tertiary companion in our simulations have the tertiary in a relatively wide orbit. We discuss the potential for detecting the presence of the tertiary companion based on LISA data in Section 4.4.

We recall that we also generated a comparative simulation where the Galactic population only follows the isolated binary channel (i.e., entirely excluding triple channels). In this simulation we obtain a total of  $\sim 9.4 \times 10^6$  double white dwarfs emitting at LISA frequencies. All results are summarized in Table 1.

In the following subsections we present our estimates for the number of individually resolvable sources and estimate the unresolved stochastic foreground. We discuss the source properties and white dwarf (core composition) types from triple systems then compare them with those from the isolated binary channel.

#### 4.1. Detectability with LISA

##### 4.1.1. Circular systems

Double white dwarfs in the LISA band are typically millions of years away from merging. They are continuous, quasi-



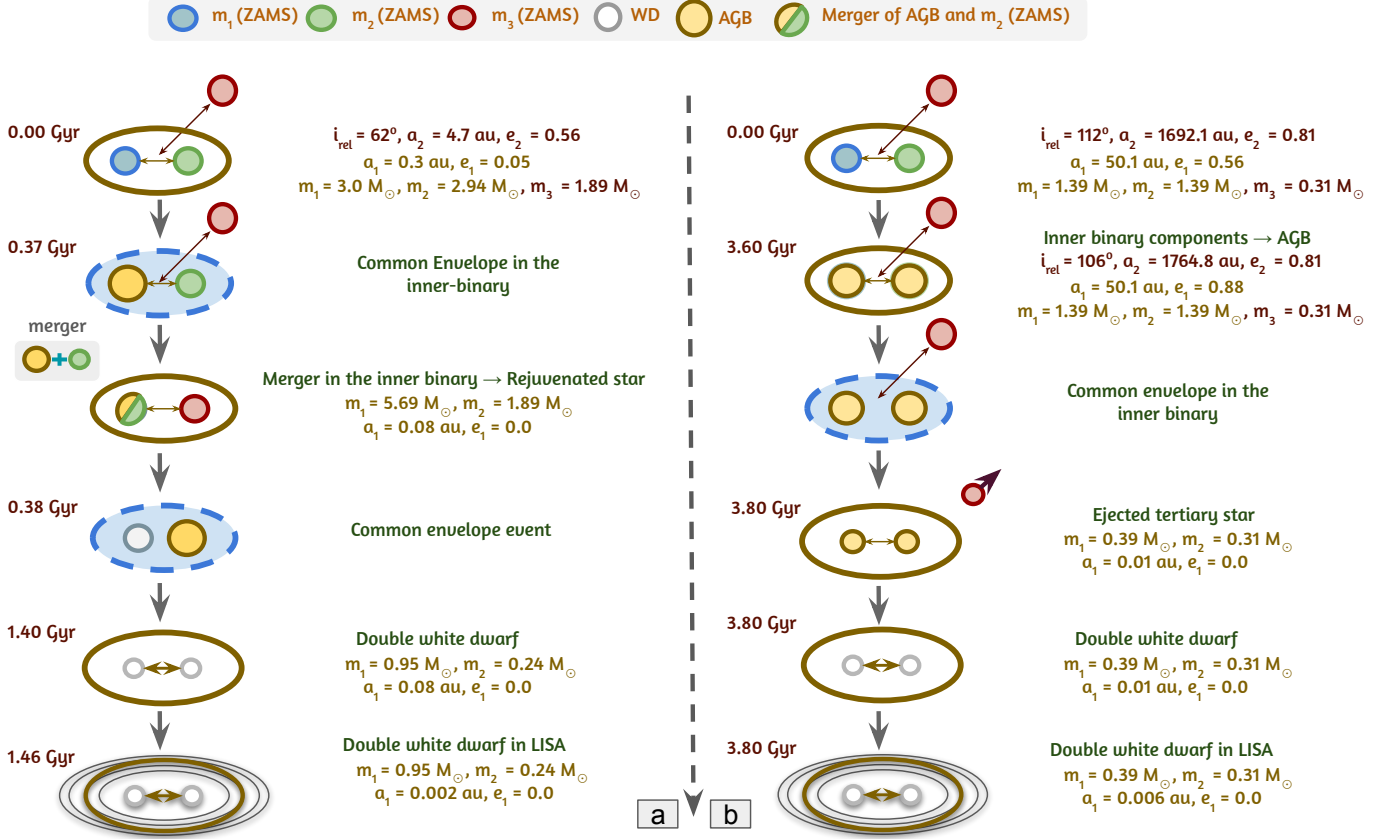


**Fig. 6.** Schematic diagrams of systems that enter the LISA frequency bandwidth after following the outer binary channel and those in which the triple eject the tertiary during the course of evolution. Panel (a) depicts an example of systems following the outer binary channel. In this scenario, the inner binary merges to form a rejuvenated star, which later enters the LISA frequency bandwidth along with the tertiary star. Panel (b) illustrates an example system that initially includes a bound third star, which facilitates a common envelope phase in the inner binary but is later ejected. The inner binary subsequently enters the LISA frequency bandwidth. The legends are similar to those in Figure 2. In addition, the yellow circle represents a star in the asymptotic giant branch (AGB) phase.

Category	$N(f < 10^{-4} \text{ Hz}) \times 10^6$	$N(\rho > 7) \times 10^3$
Triple	$7.20 \pm 0.13$	10.9
Binary	$3.80 \pm 0.10$	6.5
Triple + Binary	$11.00 \pm 0.16$	17.4
Only binaries ( $f_i = 0$ )	$9.40 \pm 0.12$	14.4

**Table 1.** The table presents the estimated counts of Galactic LISA double white dwarfs from different formation channels: Triple (originating from triple systems), Binary (originating from isolated binaries), Triple + Binary (the combined population from both channels), and Only binaries (isolated binaries with no triples, i.e., a triple fraction  $f_i = 0$ ). Errors represent scaled up the fractional Poisson error from the intrinsic population evolved with MSE.

monochromatic gravitational-wave sources for LISA. Describing these signals requires a set of eight parameters, typically chosen as  $\{\mathcal{A}_{\text{gw}}, f_{\text{gw}}, \dot{f}_{\text{gw}}, \lambda, \beta, \iota, \psi, \phi_0\}$  (LISA Consortium Waveform Working Group et al. 2023). Here,  $\mathcal{A}_{\text{gw}}$  represents the gravitational-wave amplitude,  $f_{\text{gw}}$  and  $\dot{f}_{\text{gw}}$  denote the gravitational-wave frequency and its time derivative (or chirp),  $(\lambda, \beta)$  correspond to the ecliptic longitude and latitude, respectively,  $\iota$  is the (inner) binary inclination angle with respect to the line-of-sight,  $\psi$  is the gravitational-wave polarization angle, and

$\phi_0$  represents the binary's initial phase. Our population synthesis models provide binary parameters such as component masses, orbital periods and eccentricities, sky positions and distances. We use these to derive gravitational-wave parameters as follows. As discussed above, the overwhelming majority of double white dwarfs in our simulations are circularized.

The gravitational-wave frequency of a circular binary is twice its orbital frequency  $f_{\text{orb}}$

$$f_{\text{gw}} = 2f_{\text{orb}}, \quad (3)$$

while the amplitude is given by

$$\mathcal{A}_{\text{gw}} = \frac{2(GM_c)^{5/3}}{c^4 d} (\pi f_{\text{gw}})^{2/3}, \quad (4)$$

where  $G$  and  $c$  are the gravitational constant and speed of light respectively. The amplitude is set by the source's distance  $d$  and chirp mass

$$\mathcal{M}_c = \frac{(m_1 m_2)^{3/5}}{(m_1 + m_2)^{1/5}}, \quad (5)$$

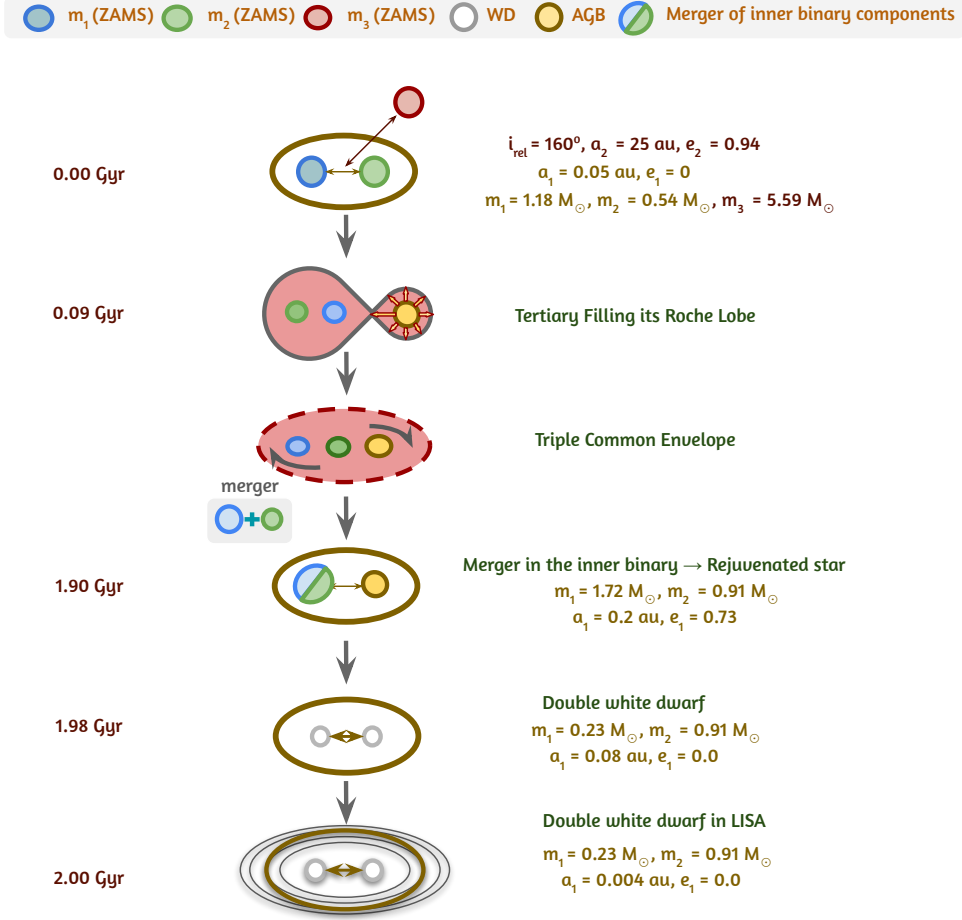


**Fig. 7.** Schematic diagram for an example system which undergoes a TCE. In this scenario, the massive star transfers mass onto the inner binary, leading to its merger and the formation of a rejuvenated star. This rejuvenated star later enters the LISA frequency bandwidth along with the tertiary star. The legends are similar to those in Figure 2. In addition, the yellow circle represents a star in the asymptotic giant branch (AGB) phase.

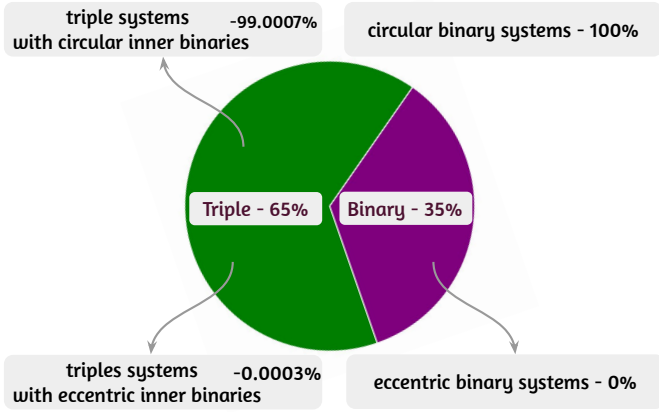


**Fig. 8.** Pie chart showing the fraction of eccentric and circular orbits among double white dwarfs from triple systems and isolated binary systems. While isolated binaries do not produce double white dwarfs with eccentric orbits, approximately  $3 \times 10^{-6}$  of LISA-detectable double white dwarfs from triple systems exhibit eccentric orbits.

The chirp mass also sets the rate at which the frequency changes due to the gravitational radiation reaction:

$$\dot{f}_{\text{gw}} = \frac{96}{5} \frac{(GM)^{5/3}}{\pi c^5} (\pi f_{\text{gw}})^{11/3}. \quad (6)$$

Equations (3), (4), and (6) define the first three parameters of the set. The ecliptic coordinates  $(\lambda, \beta)$  are inherited from the TNG50 Milky Way-like galaxy where the binary was seeded, while the remaining three parameters are assigned randomly:  $\iota$  is sampled from a uniform distribution in  $\cos \iota$ , and  $\psi$  and  $\phi_0$  are sampled from flat distributions.

As the next step, we estimate the confusion noise produced by these gravitational-wave sources in our mock Milky Way using the pipeline<sup>2</sup> described in Karnesis et al. (2021, see also Timpano et al. 2006; Crowder & Cornish 2007; Nissanke et al. 2012). The pipeline approximates the so-called “global fit” analysis, which is the currently adopted approach to handling LISA’s complex data analysis (Colpi et al. 2024, see also Littenberg & Cornish 2023; Katz et al. 2024; Deng et al. 2025). The pipeline employs a signal-to-noise ( $\rho$ ) evaluation to iteratively estimate the strain amplitude spectral density resulting from the combined signals of the unresolved (i.e., low  $\rho$ ) part of the input population. As a result, we also obtain a catalog of individually resolved (i.e., high  $\rho$ ) binaries. For our analysis, we adopt LISA’s instrumental noise requirements as defined in the technical note by LISA Science Study Team (2018). We assume a mission duration of 4 yr and use an  $\rho$  threshold of 7 to distinguish between individually resolvable LISA sources and unresolved ones, a

<sup>2</sup> <https://gitlab.in2p3.fr/Nikos/gwg>.

choice commonly adopted in detailed simulations (e.g., Crowder & Cornish 2007; Cornish & Littenberg 2007; Finch et al. 2023)

We estimate a confusion foreground from our mock population containing double white dwarf binaries from both isolated binary and triple channels to be at the level of the LISA instrument noise. We also obtain  $\sim 1.7 \times 10^4$  sources above  $\rho$  threshold, of which  $\sim 6.5 \times 10^3$  come from the isolated binaries and  $\sim 1.1 \times 10^4$  come from the triples. We illustrate these in Figure 9 (see Section 5.1 for comparison to previous works). Our estimate of the confusion noise is lower than those presented in the LISA mission proposal (Amaro-Seoane et al. 2017) and the more recent LISA Definition Study Report (Colpi et al. 2024), which used a different population synthesis study (Nelemans et al. 2004; Korol et al. 2017). This discrepancy arises from multiple aspects of population modeling, including variations in binary evolution prescriptions, Milky Way modeling, and, importantly, the inclusion of the triple formation channel in our simulations. However, since the same systematics are applied to both our triple and isolated binary populations, their differential properties remain largely unaffected. These factors collectively influence the total number of binaries in the LISA band and their properties. Identifying a single source of the difference is challenging, as these aspects are interrelated and non-trivially correlated. The LISA Consortium’s Astrophysics Working Group is currently investigating the differences and uncertainties in predicting the confusion foreground as part of the Ultra-Compact Binaries catalog comparison project (Valli et al. 2023, as well as Breivik et al. and Bobrick et al. in prep.). We refer the reader to those forthcoming results and provide a comparison using our test simulation, in which all LISA binaries were generated solely via the isolated binary channel.

#### 4.1.2. Eccentric systems

Here, we focus on eccentric systems originating from the triple formation channel. These systems were excluded from the analysis above as they are estimated to be very few (and therefore do not contribute to the overall Galactic confusion signal) and because their gravitational-wave signals differ from those of circular systems.

We find that approximately  $3 \times 10^{-6}$  of all Galactic double white dwarfs exhibit eccentric orbits. These systems result primarily from two reasons: (1) the ZLK effect excites the eccentricity of the inner binary orbit, or (2) the system becomes dynamically unstable and eventually achieves a stable configuration with high eccentricity.

In our simulations, all eccentric systems show high eccentricities ( $e > 0.9$ ) and wide semi-major axis ( $10^1 - 10^6$  au). For such orbital configurations, gravitational-wave emission predominantly occurs near pericenter passage, lasting up to a few hours and producing burst-like gravitational-wave signals. Since the orbital periods of these systems in our simulations are significantly longer than the mission duration ( $> 46$  yr), the double white dwarf burst signals will not repeat within LISA’s observation window of 4 yr.

The probability to observe a gravitational-wave burst from an individual system at periastris is  $\sim T_{\text{obs}}/T_{\text{orb}}$ , where  $T_{\text{obs}}$  is the observational time ( $\sim 4$  yr). Assuming Poisson binomial distribution, we estimate that LISA will detect at most one eccentric double white dwarf during its operational duration. Following Xuan et al. (2024), we estimate the frequency and strain ampli-

tude of such a burst signal as

$$f_{\text{burst}} \sim \frac{2}{T_{\text{orb}}(r_p)}, \quad (7)$$

$$h_{\text{burst}} = \frac{2(GM)^{5/3}}{c^4 d} \left[ \frac{2\pi}{T_{\text{orb}}(r_p)} \right]^{2/3}, \quad (8)$$

where  $r_p$  is the periastris distance. We find the (dimensionless) strain amplitudes of the gravitational-wave emitted during the periastris are between  $\sim 10^{-24}$  and  $10^{-22}$ , i.e. below the noise curve (black stars in Figure 9). Therefore, such signal would not be detectable by LISA.

#### 4.2. Population properties

In this section, we describe the similarities and differences in the population properties of double white dwarfs formed from triple systems and binary systems. Figure 10 shows the distribution of population properties such as chirp mass, primary mass, eccentricity, and gravitational-wave frequency. The green color corresponds to the properties of double white dwarfs from triple systems while the purple color shows the properties of double white dwarfs from binary star systems. The shaded green and purple regions represent the properties of resolvable double white dwarfs from triple and binary star systems, respectively. The resolved double white dwarf population traces the features of the total double white dwarf population. It is also interesting to note that all double white dwarfs in our mock Milky Way with  $f_{\text{gw}} > 2 \times 10^{-3}$  are fully resolvable by LISA. Individually resolving any double white dwarf with  $f_{\text{gw}} < 2 \times 10^{-3}$  is more difficult for LISA due to the higher degree of overlap in this frequency range.

Triple systems produce about  $\sim 1.5$  times more LISA double white dwarf systems with primary masses greater than  $0.9 M_{\odot}$  and  $\sim 3.9$  times more super-Chandrasekhar mass double white dwarfs (binary white dwarfs in which total mass of both the white dwarfs combined exceeds  $1.44 M_{\odot}$ ) than the isolated binary channel. In addition, triple systems produce  $\sim 1.6$  times more extremely low-mass white dwarfs ( $m < 0.25 M_{\odot}$ ) that enter the LISA frequency bandwidth than isolated binaries. Isolated binaries do not produce binaries with a chirp mass greater than  $0.9 M_{\odot}$ . In contrast, triple systems produce  $\sim 10^3$  binaries whose chirp mass is greater than  $0.9 M_{\odot}$ . There are two possible ways to form massive white dwarfs: 1) The system originates from a massive main-sequence progenitor that evolves to a massive white dwarf; 2) Two less massive progenitors merge to form a massive main sequence progenitor that subsequently forms a massive white dwarf. In our simulations, initial massive main-sequence progenitors are rare. Hence, it is difficult to form massive white dwarfs in isolated binaries. However, in triple systems, the two less massive progenitors in the inner binary can merge to form a massive progenitor. The merged star co-evolves with the former tertiary component to form a double white dwarf with a massive component.

There is no significant difference in the frequency distribution of double white dwarf binaries formed from isolated binaries and triple systems. This is because most double white dwarfs emerge as short-period binaries after a common envelope phase, eventually emitting gravitational waves to enter the LISA band.

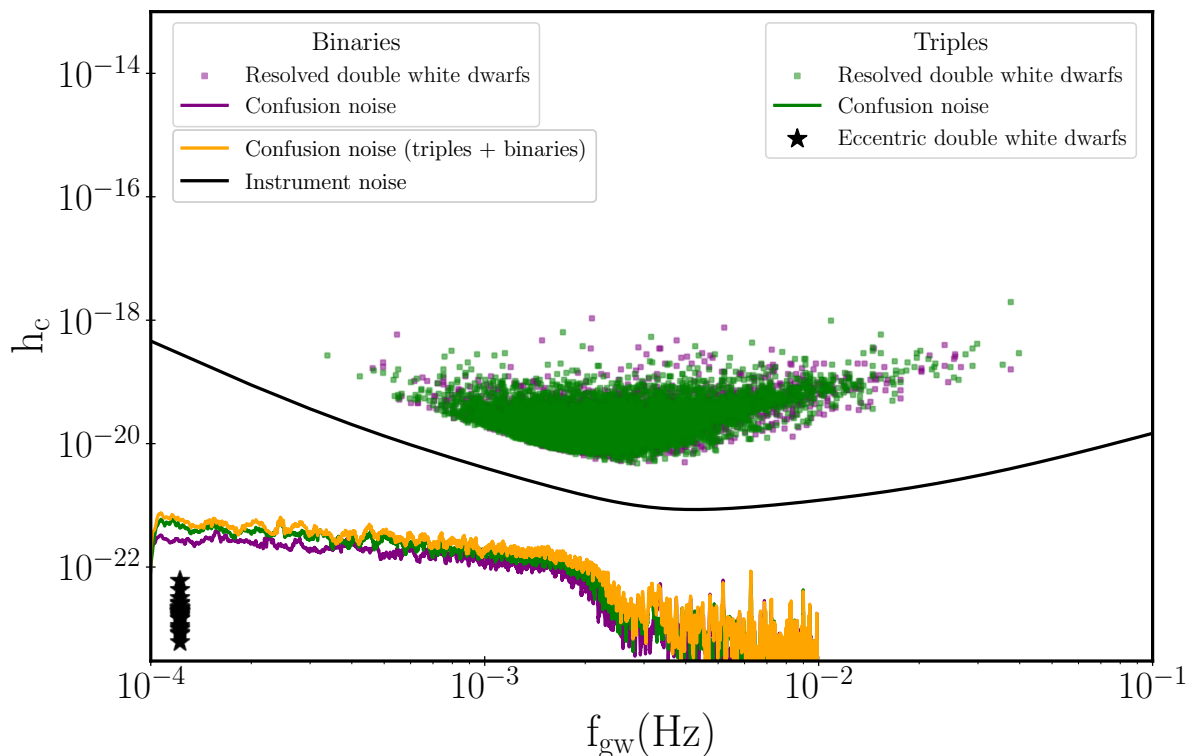


**Fig. 9.** Characteristic strain  $h_c = \mathcal{A}_{\text{gw}} \sqrt{f_{\text{gw}} T_{\text{obs}}}$  of resolved double white dwarf binaries in our mock simulation for a mission duration of  $T_{\text{obs}} = 4 \text{ yr}$ : triples in green points and isolated binary channel in purple points. This is compared to the LISA instrumental noise (black solid line). Triples with highly eccentric orbits ( $e > 0.9$ ) and other low signal-to-noise sources are marked in black and dark gray markers, respectively. The confusion background from the Galactic double white dwarf population is represented by green, purple, and orange lines for triples, binaries, and their combined contribution, respectively. All the eccentric systems (black markers) tend to have narrow periastris time ( $10^4 \text{ s}$ ) and hence they occupy a narrow frequency range. The astrophysical noise from these backgrounds remains significantly lower than the instrumental noise.

### 4.3. Different types of double white dwarfs

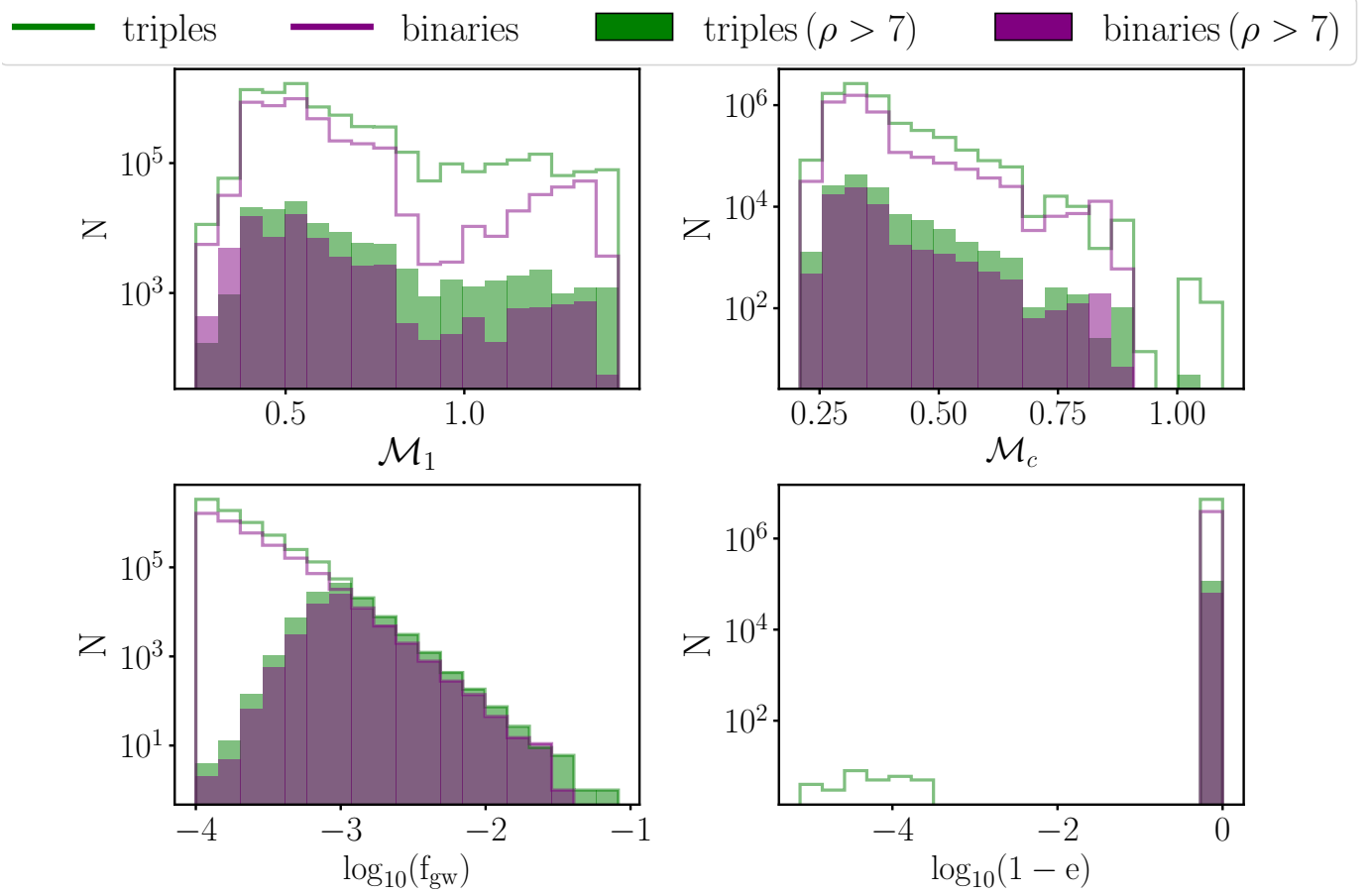
From the MSE single-star evolution model, Helium (He) white dwarfs typically originate from binary interactions where the progenitor loses its envelope before helium ignition, with typical masses of  $\lesssim 0.45 M_{\odot}$ . Carbon-Oxygen (CO) white dwarfs form from intermediate-mass stars that exhaust helium in their cores and expel their outer layers, resulting in masses between  $\sim 0.45 - 1.1 M_{\odot}$ . Oxygen-Neon (ONe) white dwarfs arise from more massive stars that undergo carbon burning before shedding their envelopes, with typical masses of  $\gtrsim 1.1 M_{\odot}$ .

Figure 11 shows the relative numbers of different double white dwarf (core composition) types from binary and triple systems, respectively. Our simulations produce all types of double white dwarfs in the LISA frequency bandwidth from both triple and binary star systems, including He-He, He-CO, He-ONe, CO-CO, and CO-ONe systems. He-CO systems dominate the population of double white dwarfs originating from both triples and isolated binaries. Our simulations produce ONe-ONe systems only from the triple populations, but the sampling uncertainties in this mass range are too high to draw meaningful conclusions.

### 4.4. Detectability of the third star

We enfranchise again that approximately 57% of all double white dwarfs detectable by LISA will have a bound tertiary companion. The bound tertiary star can be found in various evolutionary stages, including as a main sequence star, a giant star, or a white dwarf. In the remaining 43% of systems, the third star either became unbound or there was a merger of two stars, reducing the system from a triple to a binary (cf. Section 3.3). If the tertiary is retained, it can impart accelerations to the center of mass of the binary, leading to observable Doppler shifts in the gravitational-wave signals (e.g., Seto 2008; Robson et al. 2018; Tamanini & Danielski 2019).

In the context of LISA Galactic binaries in hierarchical triple systems, Robson et al. (2018) identifies three regimes, essentially governed by the ratio of the outer orbital period to the observation time: 1) When the outer period is much larger than the observation time the hierarchical orbit imparts an overall unobservable Doppler shift. 2) When the outer period is up to a factor ten larger than the observation time the influence of the companion can be detected. 3) When the outer period is shorter than or comparable to the observation time, the eccentricity and period of the hierarchical orbit can be inferred. Specifically, a tertiary companion leaves a detectable imprint in the gravitational-wave



**Fig. 10.** Population properties of LISA-detectable double white dwarfs from triple systems compared to isolated binaries. Overall, triple systems produce more massive white dwarfs than isolated binaries. For more details, see Section 4.2.

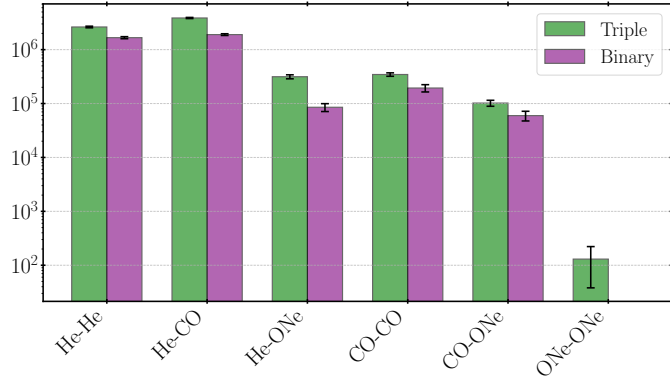


**Fig. 11.** Types of LISA-detectable double white dwarfs formed from triple systems compared to isolated binaries. In our models, ONe-ONe double white dwarfs are produced exclusively in triple systems. Error bars represent scaled up the fractional Poisson error from the intrinsic population evolved with MSE.

signal if the outer binary period satisfies:

$$T_2 \lesssim T_{\text{lim}} = 43.2 \text{ yr} \left( \frac{\rho}{10} \cdot \frac{m_3}{1.0 M_\odot} \cdot \frac{f}{5 \text{ mHz}} \right)^{3/4} \left( \frac{m_1 + m_2}{2 M_\odot} \right)^{-1/2} \times \left( \frac{T_{\text{obs}}}{4 \text{ yr}} \right)^{3/8} \left( \frac{1 + \frac{1}{2} e_2^2}{(1 - e_2^2)^{5/2}} \right)^{3/8},$$

(9)

where  $\rho$  is the signal-to-noise ratio of the binary.

In our simulations, in all systems that have retained the tertiary companion, the outer orbits are too wide to have any detectable effect within the resulting LISA gravitational-wave signal. Figure 12 compares the outer orbital period  $T_2$  with the factor on the right hand side of the Eq. (9). The black line shows the limit where  $T_2$  equals the factor on the right hand side. We find that none of our surviving triple systems lie within, or close to, the detectable limit. In addition, we find no systems where  $T_{\text{orb}} \leq T_{\text{obs}}$  or  $T_{\text{orb}} \approx 10 \times T_{\text{obs}}$ . The minimum outer semi-major axis across all systems is found to be approximately 21 au, which corresponds to an orbital period of around 63 yr.

## 5. Discussion

We discuss our results in the context of previous works, present the uncertainties associated with our models, and describe the constraints imposed by electromagnetic observations.

### 5.1. Comparison to previous works

We calculated the number and population properties of LISA double white dwarfs that originated from triple systems (cf. Section 2). We also simulated LISA double white dwarfs from an isolated binary population (cf. Appendix A) to compare with triple populations. Our isolated binary simulation predicts  $\approx 10^4$

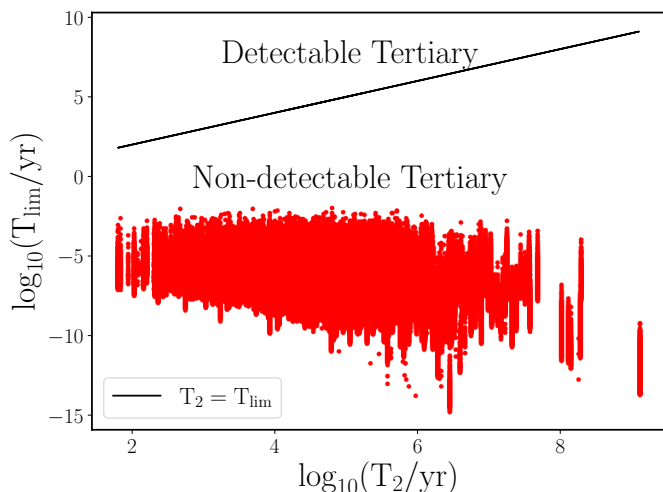


**Fig. 12.** Comparison between the outer orbital period of a triple system and the factor on the right-hand side of Eq. (9). Red points represent  $T_{\text{lim}}$  vs outer orbital period  $T_2$  for all the Galactic LISA double white dwarfs with a bound third star. The black line represents the points where  $T_2 = T_{\text{lim}}$ . No tertiary star satisfies Eq. (9) for detectability within the LISA frequency bandwidth.

individually resolvable double white dwarfs in the LISA frequency bandwidth, which agrees with previous works, including Nelemans et al. (2004); Ruiter et al. (2010); Yu & Jeffery (2010); Korol et al. (2017); Lamberts et al. (2019); Li et al. (2023); Thiele et al. (2023); Tang et al. (2024). In total, our models predict  $\sim 1.1 \times 10^7$  double white dwarf sources that emit gravitational waves in the LISA frequency bandwidth but have very low  $\rho$  to be individually detected by LISA.

In particular, Korol et al. (2017) used binary population model of Toonen et al. (2012) based on the SeBa binary population synthesis code (Portegies Zwart & Verbunt 1996) and an analytic Galactic potential and star formation history to estimate the number of Galactic double white dwarfs. They predict  $\sim 2.6 \times 10^7$  LISA double white dwarfs as foreground noise and  $\sim 2.5 \times 10^4$  as individually resolvable LISA double dwarf sources. Korol et al. (2022) performed a data-driven analysis using existing observational double white dwarf data and also estimated a LISA double white dwarf population of  $\sim 2.6 \times 10^7$  as foreground noise and  $\sim 6.0 \times 10^4$  as individually resolvable LISA double dwarf sources. Using the BSE code (i.e. same as out isolated binary evolution channel but with different underlying assumptions) combined with the Fire cosmological simulation, Lamberts et al. (2019) constructed the Galactic LISA double white dwarf population and estimated  $\sim 6.2 \times 10^7$  double white dwarf sources as foreground noise and  $\sim 1.2 \times 10^4$  as individually resolvable LISA double dwarf sources. Further, Li et al. (2023) also used the BSE code but with a mass transfer stability criterion by adopting critical mass ratios from the adiabatic mass loss model and estimated a foreground LISA double white dwarf population size of  $\sim 5.0 \times 10^7$  and about  $4.0 \times 10^4$  individually resolvable double white dwarfs. Our results are broadly consistent with previous studies in terms of the number of resolved binaries, but we estimate comparatively fewer double white dwarf sources emitting gravitational waves in the LISA frequency band (see Section 4.1.1 for details). This discrepancy may arise from multiple factors, including the use of different population synthesis codes, varying assumptions underlying binary evolution, and different approaches to modeling the Galaxy. Most importantly,

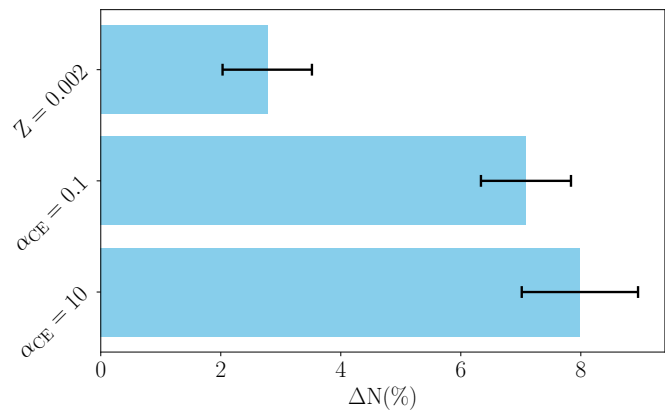


**Fig. 13.** Fractional difference of LISA-detectable double white dwarfs from models with varying common envelope efficiency,  $\alpha_{\text{CE}}$ , and subsolar metallicity, relative to the default values ( $\alpha_{\text{CE}} = 1$ ,  $Z = 0.02$ ). The number of double white dwarfs varies by up to 8% when the common envelope parameters are modified. Error bars represent scaled up the fractional Poisson error from the intrinsic population evolved with MSE.

previous studies model isolated binary evolution only, ignoring triple evolution channel.

When comparing our isolated binary evolution results (with triple fraction set to zero, see Table 1) to previous studies, several factors can contribute to differences in LISA predictions. For instance, assuming a different total stellar mass for the Milky Way would linearly scale our results (cf. Eq. 2). As shown by Keim et al. (2023), the underlying star formation history also plays a role (see also Yu & Jeffery 2010). However, the most likely primary source of differences is the modeling of stellar and binary evolution. This was recently demonstrated by van Zeist et al. (2024), who investigated the gravitational-wave population of the Large and Small Magellanic Clouds as a case study using the BPASS (Eldridge et al. 2017) and SeBa codes. They specifically attributed variations in the predicted number of LISA double white dwarfs to differences in the treatment of CE evolution and the stability of mass transfer. Indeed, even studies using the same population synthesis code report significant differences in LISA predictions when these processes are modeled differently (e.g., Korol et al. 2017; Li et al. 2023). As mentioned before, quantifying the impact of all these factors on LISA predictions is a large collaborative effort within the LISA Consortium’s Astrophysics Working Group. We refer the reader to those forthcoming results.

## 5.2. Uncertainties in our modelling

In our normalization calculations, we assume constant multiplicity fractions 0.2, 0.3, and 0.5 for stars in triple, binary, and single systems respectively. The multiplicity fractions play a crucial role in the mass normalization and, hence, the total number of LISA double dwarfs. All previous works assume a zero triple fraction. To compare our results with previous works, we have also calculated the number of LISA double dwarfs with a 0.5 binary fraction and zero triple fraction. We found  $\sim 9 \times 10^6$  systems, showing consistency with previous studies in scale. For the same isolated binary population, assuming a 0.2 triple fraction, we only obtain  $\sim 3.8 \times 10^6$  systems, half as many. This highlights the sensitivity of the results to the assumed multiplicity fraction.

We use a critical mass ratio criterion to model the stability of mass transfer. Studies employing alternative stability criteria find

that relatively fewer systems undergo a common envelope phase (Tauris et al. 2000; Podsiadlowski et al. 2002; Ge et al. 2010; Woods et al. 2011; Passy et al. 2012; Ge et al. 2015, 2020; Temmink et al. 2023; Li et al. 2023; van Zeist et al. 2024). Additionally, we assume that the orbit circularizes following the common envelope phase. However, there is ongoing debate about whether residual eccentricity may persist at the end of the common envelope evolution. The modeling of unstable mass transfer leading to a common envelope phase follows the approximate  $\alpha$ - $\lambda$  formalism. We investigated the effect of the common envelope efficiency parameter,  $\alpha_{\text{CE}}$ , on our results. For lower ( $\alpha_{\text{CE}} = 0.1$ ) and higher efficiency parameters ( $\alpha_{\text{CE}} = 10$ ), our simulations yield approximately  $7.5 \times 10^6$  and  $7.6 \times 10^6$  LISA double white dwarfs, respectively. For a lower value of the common envelope efficiency, the common envelope phase is relatively more effective at shrinking the orbit. Consequently, these systems enter the LISA frequency bandwidth within a Hubble time. In contrast, for the default value ( $\alpha_{\text{CE}} = 1$ ), the common envelope phase results in a relatively wider orbital period. However, for a high common envelope efficiency parameter, there is an increase in the number of LISA-detectable double white dwarf binaries. This is because the more efficient common envelope phase is less likely to merge binaries that would otherwise have merged for  $\alpha_{\text{CE}} = 1$ .

We assume that all progenitors of the Galactic LISA double white dwarfs are formed with solar metallicity. About  $\sim 2\%$  of the star particles in the selected Milky Way model have subsolar metallicity. However, our Galaxy encompasses a larger range of metallicities. We also explore the impact of sub-solar metallicity by constructing the galaxy using the procedure described in Section 2.3 but with an initial metallicity of  $Z = 0.0002$ . It results in approximately  $\sim 7.5 \times 10^6$  LISA double white dwarfs, an increase of  $\sim 0.3 \times 10^6$  compared to those with solar metallicity. Stars with lower metallicity evolve relatively faster. For example, a  $0.91 M_{\odot}$  star evolves into a white dwarf within a Hubble time at sub-solar metallicity, whereas it does not at solar metallicity. This increase in the number of low-mass stars that evolve into white dwarfs significantly contributes to the population of LISA-detectable double white dwarfs.

The ZLK effect induces eccentric oscillations in the inner binary, increasing the possibility of mass transfer at periapsis or eccentric mass transfer. The MSE model treats eccentric mass transfer using an approximate prescription. Furthermore, MSE also uses approximate prescriptions for mass transfer from the third star onto the inner binary. In our simulation, about  $5.5\%$  of Galactic LISA double white dwarfs undergo a TCE phase before reaching the LISA frequency bandwidth. Inputs from detailed hydrodynamical (Glanz & Perets 2020) simulations of eccentric mass transfer and triple mass transfer are needed to improve the eccentric mass transfer and TCE prescriptions.

We highlight that simulations of triple systems are computationally expensive. We simulated  $10^5$  triple systems, producing  $\sim 3 \times 10^3$  LISA double white dwarfs. Deriving from the mass function in Figure 1, there is a very low probability of producing high-mass white dwarfs. Hence, uncertainties in the statistics on the number of white dwarfs increase with mass. There is also a possibility of producing One white dwarfs from 8-10  $M_{\odot}$  stars. Our models are created from progenitors in the mass range 1-8  $M_{\odot}$ . The sampling uncertainties in this mass range are too high to draw meaningful conclusions. In addition, we use random sampling to construct the initial triple population. However, more targeted sampling algorithms, such as STROOPWAFEL (Broekgaarden et al. 2019), could be employed to assess the impact of sampling uncertainties in the initial population on rare events.

Finally, we note that MSE is a population synthesis code designed for statistical studies, and individual system modeling is not recommended. Due to variations in floating-point representation and rounding across different machines, the code may yield slightly different results when executed on different machines. However, these numerical difficulties average out on a large sample of the population. Given this inherent complexity, we limited the computational time to 10 hours per system. Within this time frame,  $4\%$  systems did not complete their evolution. Of these, around  $0.4\%$  were dynamically unstable, while the remaining systems were undergoing stable secular evolution. The majority of systems completed their evolution in under 2 hours. Additionally, only  $0.1\%$  systems had white dwarfs or both components massive enough to evolve into white dwarfs within a Hubble time. These systems were included in error calculations, while the remaining incomplete systems were excluded without affecting the overall results.

### 5.3. Possibility of electromagnetic constraints to LISA observations

While millions of double white dwarfs will emit gravitational waves in the LISA frequency bandwidth, only a few hundred double white dwarfs are well-characterized in electromagnetic observations (e.g., Munday et al. 2023). Of these, 48 of the binaries will have a high  $\rho$  ratio and will serve as verification binaries for the LISA mission (e.g., Stroeer & Vecchio 2006; Kupfer et al. 2018, 2024; Finch et al. 2023). To date, it is unknown if any of these known LISA binaries are part of triple systems with wide tertiary companion.

LISA is set to be launched in 2035 (Colpi et al. 2024). However, some electromagnetic observations/surveys planned in the near future will already increase the sample of short-period double white dwarfs and offer better constraints for the modeling, data analysis, and detection techniques of LISA double white dwarfs. This includes new binary insights from Gaia's next data release (DR4), SDSS-V (Kervella et al. 2017), LAMOST (Zhao et al. 2012), ZTF, 4MOST (de Jong et al. 2019), WEAVE (de Vries et al. 2014), the Asteroid Terrestrial-impact Last Alert System (Heintz et al. 2018; Tonry et al. 2018), the Gravitational-wave Optical Transient Observer (Steehhs et al. 2022), Euclid (Laureijs et al. 2011), the Nancy Roman Space Telescope (?), and Vera Rubin-LSST (Collaboration et al. 2009).

Similarly to the approach taken by Heintz et al. (2024), who used the age discrepancy from observational data to quantify the contribution of triple systems, applying comparable modeling techniques to forthcoming double white dwarf observations could provide further constraints on the contribution of triples to double white dwarfs in the LISA frequency bandwidth.

## 6. Conclusion

We estimated the Galactic LISA double white dwarfs from triple systems. We combined the triple population synthesis code MSE and the TNG50 cosmological simulations to seed a Milky Way-like galaxy to obtain a population of LISA-detectable double white dwarfs. To compare our results with LISA double white dwarfs from isolated binaries, we also estimated the LISA double white dwarf population from isolated binaries using the same MSE code. The main conclusions are listed below:

1. Galactic LISA double white dwarfs have comparable contributions from both binary and triple channels. We estimate  $\sim 7.2 \times 10^6$  and  $\sim 3.8 \times 10^6$  LISA double white dwarfs from

triple and binary star systems, respectively. Of these systems,  $\sim 1.09 \times 10^4$  and  $\sim 6.5 \times 10^3$  are individually resolvable double white dwarfs from triple and binary star systems, respectively. In addition, we find that the confusion foreground produced from our population (triples and isolated binaries) is below the instrument noise level.

2. We identify five different key processes that shape the evolutionary pathways of triple systems, leading to the formation of double white dwarfs that emit gravitational waves in the LISA frequency bandwidth.
  - (a) Induced mass transfer: the gravitational perturbations from the third star triggers a mass transfer episode in the inner binary that leads to a shorter orbital period.
  - (b) Outer binary channel: the inner binary merges to form a rejuvenated star that combines with the third star to enter the LISA frequency bandwidth.
  - (c) Ejected tertiary: perturbations from the third star alter the inner binary configurations and are responsible for the short period of the inner binary, but the third star is later ejected before the inner binary enters the LISA frequency bandwidth.
  - (d) Triple common envelope: Mass transfer from the tertiary star onto the inner binary that eventually brings the inner binary closer to short orbital periods.
  - (e) Inner binary channel: A binary with a third star that is too distant to have any effect, enters the LISA frequency bandwidth due to effectively isolated binary interactions.
3. Our models show no major distinguishable differences in the population properties of systems originating from triples compared to those from isolated binaries.
4. Of the LISA double white dwarfs from triple systems, about  $\sim 50\%$  of systems have a bound third star. However, the tertiary is typically too distant to have an observable imprint in the gravitational-wave signal of the inner binary.
5. Of the predicted LISA double white dwarfs from triple systems, we estimate that the majority of systems which enter the LISA frequency bandwidth have circular orbits, and only  $3 \times 10^{-6}$  (i.e. 31 systems in total in the Milky Way) of these systems have eccentric orbits. Meanwhile, in the estimated LISA double white dwarf population from isolated binary star systems, all systems have circular orbits. All the eccentric systems are found to have highly eccentric orbits ( $e > 0.9$ ) and will emit gravitational bursts, with a typical periastron period of a few hours. However, they are unlikely to be observable due to their small gravitational-wave strain amplitude.
6. In our Galactic LISA double white dwarf population, we observe all types of double white dwarfs, with He-CO double white dwarfs being the dominant configuration.

Our study is the first to investigate the role of the triple evolution channel in the context of future LISA observations. We quantitatively assess the impact of including this channel on the number of observable LISA sources. While our results indicate no major distinguishable differences in the population properties of systems originating from triples compared to those formed through isolated binary evolution, they are particularly relevant for the future interpretation of LISA data on the Galactic population. Additionally, we show that the triple channel produces highly eccentric sources—although rare, these systems generate burst-like signals, in contrast to the predominantly monochromatic continuous signals emitted by the majority of the Galactic population. Thus, it is also important to consider these systems in the context of LISA data analysis.

*Acknowledgements.* ASR would like to thank Adrian Hamers for his guidance on the fundamentals of triple dynamics and the development of the MSE code, which was instrumental in this work. ASR also thanks Nikolaos Karnesis for constructing the confusion background using our population. JS, SJ, and SDM acknowledge funding from the Netherlands Organisation for Scientific Research (NWO), as part of the Vidi research program BinWaves (project number 639.042.728, PI: de Mink). ST also acknowledges support from the Netherlands Research Council NWO (VENI 639.041.645 and VIDI 203.061 grants). **Software:** MSE (Hamers et al. 2021), Matplotlib (Hunter 2007), NumPy (van der Walt et al. 2011), pandas (McKinney 2010), gwg (Karnesis et al. 2021). *Data availability:* All the codes used in this projects are available at [GitHub repository](#). The data produced during this study is available upon request.



## Appendix A: LISA double white dwarfs from isolated binary population

This section explains how we seed the double white dwarfs from isolated binary channels to a Milky Way-like galaxy. We do it in two steps.

In the first step, we construct a synthetic population of isolated zero-age-main-sequence binaries in the first step. The primary mass ( $m_1$ ) is sampled from Kroupa's IMF (Kroupa 2001). Following this, we sample the orbital period of these binaries following empirically derived functions from Moe & Di Stefano (2017). Using  $m_1$  and  $T_1$ , we sample the initial mass ratio and eccentricities using functions from Moe & Di Stefano (2017). This mass ratio is then used to calculate  $m_2$ . For a fair comparison to the triple systems, all masses are restricted to be between  $1 - 8 M_\odot$ . Furthermore, we reject any systems that are Roche lobe filling (Eggleton 1983). We note that this population inherently differs from the inner binaries of triple systems. The crucial, though not the only, distinction arises from the dynamical stability requirement in triples, which forces the inner binary to be more compact. As a result, the semi-major axis distribution of inner binaries in triples is significantly more compact compared to that of isolated binaries. We repeat the process described in Sec 2.3 to create a population of  $10^5$  isolated binaries. Based on Figure 1 we note that this isolated binary population looks distinctly different from the inner binary population of the triple systems. We evolve this synthetic population until Hubble time using MSE and select the double white dwarf that enters LISA frequency bandwidth.

In the second step, We use the same galaxy and a similar method as mentioned in Section 2.3 to seed the LISA double white dwarfs in the Galaxy. However, the total stellar mass in the simulated population is calculated after using an isolated binary population and is given by:

$$M_{\text{tot, MSE}} = \frac{N_{b, \text{in range}}}{f_{b, \text{in range}} \cdot f_b} \cdot [f_t \cdot m_t + f_b \cdot m_b + (1 - f_t - f_b) \cdot m_s], \quad (\text{A.1})$$

where  $N_{b, \text{in range}} = 10^5$  is the number of simulated isolated binary-star systems with MSE,  $f_{b, \text{in range}}$  is the fraction of binaries in this range relative to the full mass range, and  $f_t = 0.2$ ,  $f_b = 0.3$ , and  $1 - f_t - f_b = 0.5$  represent the fractions of triples, binaries, and singles in the full stellar population;  $m_t = 3.5 M_\odot$ ,  $m_b = 0.9 M_\odot$ , and  $m_s = 0.5 M_\odot$  denote the average masses of triple, binary, and single systems, respectively.

## References

Amaro-Seoane, P., Andrews, J., Arca Sedda, M., et al. 2023, *Living Reviews in Relativity*, 26, 2  
Amaro-Seoane, P., Audley, H., Babak, S., et al. 2017, arXiv e-prints, arXiv:1702.00786  
Antonini, F., Toonen, S., & Hamers, A. S. 2017, *ApJ*, 841, 77  
Bland-Hawthorn, J. & Gerhard, O. 2016, *ARA&A*, 54, 529  
Broekgaarden, F. S., Justham, S., de Mink, S. E., et al. 2019, *Monthly Notices of the Royal Astronomical Society*, 490, 5228–5248  
Collaboration, L. S. et al. 2009, arXiv e-prints [0912.0201]  
Colpi, M., Danzmann, K., Hewitson, M., et al. 2024, arXiv e-prints, arXiv:2402.07571  
Comerford, T. A. F. & Izzard, R. G. 2020, *MNRAS*, 498, 2957  
Cornish, N. J. & Littenberg, T. B. 2007, *Physical Review D*, 76  
Crowder, J. & Cornish, N. J. 2007, *Phys. Rev. D*, 75, 043008  
Danielski, C., Korol, V., Tamanini, N., & Rossi, E. M. 2019, *A&A*, 632, A113  
de Jong, R. S., Agertz, O., Berbel, A. A., et al. 2019, *The Messenger*, 175, 3  
de Vries, N., Portegies Zwart, S., & Figueira, J. 2014, *MNRAS*, 438, 1909  
Deng, S., Babak, S., Jeune, M. L., et al. 2025, *Modular global-fit pipeline for LISA data analysis*

Eggleton, P. P. 1983, *ApJ*, 268, 368  
Eggleton, P. P. & Kiseleva-Eggleton, L. 2001, *The Astrophysical Journal*, 562, 1012  
Eggleton, P. P. & Tokovinin, A. A. 2008, *MNRAS*, 389, 869  
Eldridge, J. J., Stanway, E. R., Xiao, L., et al. 2017, *PASA*, 34, e058  
Fabrycky, D. & Tremaine, S. 2007, *ApJ*, 669, 1298  
Faherty, J. K., Burgasser, A. J., Bochanski, J. J., et al. 2011, *AJ*, 141, 71  
Finch, E., Bartolucci, G., Chucherko, D., et al. 2023, *MNRAS*, 522, 5358  
Ge, H., Hjellming, M. S., Webbink, R. F., Chen, X., & Han, Z. 2010, *The Astrophysical Journal*, 717, 724  
Ge, H., Webbink, R. F., Chen, X., & Han, Z. 2015, *The Astrophysical Journal*, 812, 40  
Ge, H., Webbink, R. F., Chen, X., & Han, Z. 2020, *The Astrophysical Journal*, 899, 132  
Glanz, H. & Perets, H. B. 2020, *Monthly Notices of the Royal Astronomical Society*, 500, 1921  
Grishin, E. & Perets, H. B. 2022, *MNRAS*, 512, 4993  
Hamers, A. S. & Dosopoulou, F. 2019, *ApJ*, 872, 119  
Hamers, A. S., Glanz, H., & Neunteufel, P. 2022, *ApJS*, 259, 25  
Hamers, A. S., Pols, O. R., Claeys, J. S. W., & Nelemans, G. 2013, *MNRAS*, 430, 2262  
Hamers, A. S., Rantala, A., Neunteufel, P., Preece, H., & Vynatheya, P. 2021, *MNRAS*, 502, 4479  
Hamers, A. S. & Thompson, T. A. 2019, *ApJ*, 882, 24  
Heintz, T. M., Hermes, J. J., Tremblay, P. E., et al. 2024, *ApJ*, 969, 68  
Heinze, A. N., Tonry, J. L., Denneau, L., et al. 2018, *AJ*, 156, 241  
Hunter, J. D. 2007, *Computing in Science and Engineering*, 9, 90  
Hurley, J. R., Pols, O. R., & Tout, C. A. 2000, *MNRAS*, 315, 543  
Hurley, J. R., Tout, C. A., & Pols, O. R. 2002, *MNRAS*, 329, 897  
Iben, Jr., I. & Livio, M. 1993, *PASP*, 105, 1373  
Iben, I., J. & Tutukov, A. V. 1984, *ApJS*, 54, 335  
Ivanova, N., Justham, S., Chen, X., et al. 2013, *A&A Rev.*, 21, 59  
Jiang, Y.-F. & Tremaine, S. 2010, *MNRAS*, 401, 977  
Kang, Y., Liu, C., & Shao, L. 2021, *AJ*, 162, 247  
Karnesis, N., Babak, S., Pieroni, M., Cornish, N., & Littenberg, T. 2021, *Phys. Rev. D*, 104, 043019  
Katz, B., Dong, S., & Malhotra, R. 2011, *Phys. Rev. Lett.*, 107, 181101  
Katz, M. L., Danielski, C., Karnesis, N., et al. 2022, *MNRAS*, 517, 697  
Katz, M. L., Karnesis, N., Korsakova, N., Gair, J. R., & Stergioulas, N. 2024, *An efficient GPU-accelerated multi-source global fit pipeline for LISA data analysis*  
Keim, M. A., Korol, V., & Rossi, E. M. 2023, *MNRAS*, 521, 1088  
Kervella, P., Thévenin, F., & Lovis, C. 2017, *A&A*, 598, L7  
Kiseleva, L. G., Eggleton, P. P., & Mikkola, S. 1998, *Monthly Notices of the Royal Astronomical Society*, 300, 292  
Korol, V., Hallakoun, N., Toonen, S., & Karnesis, N. 2022, *MNRAS*, 511, 5936  
Korol, V., Rossi, E. M., Groot, P. J., et al. 2017, *MNRAS*, 470, 1894  
Kozai, Y. 1962, *AJ*, 67, 591  
Kroupa, P. 2001, *MNRAS*, 322, 231  
Kupfer, T., Korol, V., Littenberg, T. B., et al. 2024, *ApJ*, 963, 100  
Kupfer, T., Korol, V., Shah, S., et al. 2018, *MNRAS*, 480, 302  
Lamberts, A., Blunt, S., Littenberg, T. B., et al. 2019, *MNRAS*, 490, 5888  
Laureijs, R., Amiaux, J., Arduini, S., et al. 2011, arXiv e-prints [1110.3193]  
Li, Z., Chen, X., Ge, H., Chen, H.-L., & Han, Z. 2023, *A&A*, 669, A82  
Lidov, M. L. 1962, *Planet. Space Sci.*, 9, 719  
Lillo-Box, J., Ribas, Á., Montesinos, B., et al. 2021, *A&A*, 653, A40  
LISA Consortium Waveform Working Group, Afshordi, N., Akçay, S., et al. 2023, arXiv e-prints, arXiv:2311.01300  
LISA Science Study Team. 2018, *LISA Science Requirements Document*, Tech. Rep. ESA-L3-EST-SCI-RS-001, ESA, [www.cosmos.esa.int/web/lisa/lisa-documents/](http://www.cosmos.esa.int/web/lisa/lisa-documents/)  
Littenberg, T. B. & Cornish, N. J. 2023, *Physical Review D*, 107  
Livio, M. & Soker, N. 1988, *ApJ*, 329, 764  
Mardling, R. A. & Aarseth, S. J. 2001, *MNRAS*, 321, 398  
Maxted, P. F. L., Marsh, T. R., Moran, C. K. J., & Han, Z. 2000, *Monthly Notices of the Royal Astronomical Society*, 314, 334  
McKinney, W. 2010, in *Proceedings of the 9th Python in Science Conference (SciPy 2010)*, 51–56  
Michaely, E. & Perets, H. B. 2014, *ApJ*, 794, 122  
Moe, M. & Di Stefano, R. 2017, *ApJS*, 230, 15  
Munday, J., Marsh, T. R., Hollands, M., et al. 2023, *MNRAS*, 518, 5123  
Nelemans, G., Yungelson, L. R., & Portegies Zwart, S. F. 2004, *MNRAS*, 349, 181  
Nelson, D., Pillepich, A., Springel, V., et al. 2019, *MNRAS*, 490, 3234  
Nissanke, S., Vallisneri, M., Nelemans, G., & Prince, T. A. 2012, *ApJ*, 758, 131  
Offner, S. S. R., Moe, M., Kratter, K. M., et al. 2023, in *Astronomical Society of the Pacific Conference Series*, Vol. 534, *Protostars and Planets VII*, ed. S. Inutsuka, Y. Aikawa, T. Muto, K. Tomida, & M. Tamura, 275  
Paczynski, B. 1976, in *IAU Symposium*, Vol. 73, *Structure and Evolution of Close Binary Systems*, ed. P. Eggleton, S. Mitton, & J. Whelan, 75

- Pagel, B. E. J. 1997, *Nucleosynthesis and Chemical Evolution of Galaxies*
- Passy, J.-C., Herwig, F., & Paxton, B. 2012, *The Astrophysical Journal*, 760, 90
- Perets, H. B. & Kratter, K. M. 2012, *ApJ*, 760, 99
- Perpinyà-Vallès, M., Rebassa-Mansergas, A., Gänsicke, B. T., et al. 2019, *MNRAS*, 483, 901
- Pillepich, A., Nelson, D., Springel, V., et al. 2019, *MNRAS*, 490, 3196
- Podsiadlowski, P., Rappaport, S., & Pfahl, E. D. 2002, *The Astrophysical Journal*, 565, 1107
- Portegies Zwart, S. F. & Verbunt, F. 1996, *A&A*, 309, 179
- Raghavan, D., McAlister, H. A., Henry, T. J., et al. 2010, *ApJS*, 190, 1
- Rajamuthukumar, A. S., Hamers, A. S., Neunteufel, P., Pakmor, R., & de Mink, S. E. 2023, *ApJ*, 950, 9
- Ransom, S. M., Stairs, I. H., Archibald, A. M., et al. 2014, *Nature*, 505, 520
- Rantala, A., Pihajoki, P., Mannerkoski, M., Johansson, P. H., & Naab, T. 2020, *MNRAS*, 492, 4131
- Rebassa-Mansergas, A., Xu, S., Raddi, R., et al. 2022, *ApJ*, 927, L31
- Rivinius, T., Baade, D., Hadrava, P., Heida, M., & Klement, R. 2020, *A&A*, 637, L3
- Robson, T., Cornish, N. J., Tamanini, N., & Toonen, S. 2018, *Phys. Rev. D*, 98, 064012
- Ruiter, A. J., Belczynski, K., Benacquista, M., Larson, S. L., & Williams, G. 2010, *ApJ*, 717, 1006
- Seto, N. 2008, *ApJ*, 677, L55
- Shappee, B. J. & Thompson, T. A. 2013, *ApJ*, 766, 64
- Shariat, C., Naoz, S., El-Badry, K., et al. 2024, *arXiv e-prints*, arXiv:2407.06257
- Steehls, D., Galloway, D. K., Ackley, K., et al. 2022, *MNRAS*, 511, 2405
- Stegmann, J., Antonini, F., & Moe, M. 2022a, *MNRAS*, 516, 1406
- Stegmann, J., Antonini, F., Schneider, F. R. N., Tiwari, V., & Chattopadhyay, D. 2022b, *Phys. Rev. D*, 106, 023014
- Stegmann, J., Vigna-Gómez, A., Rantala, A., et al. 2024, *Astrophys. J. Lett.*, 972, L19
- Stroeer, A. & Vecchio, A. 2006, *Classical and Quantum Gravity*, 23, S809
- Tamanini, N. & Danielski, C. 2019, *Nature Astronomy*, 3, 858
- Tang, P., Eldridge, J., Meyer, R., et al. 2024, *arXiv e-prints*, arXiv:2405.20484
- Tauris, T. M., den Heuvel, E. P. J. v., & Savonije, G. J. 2000, *Astrophys. J. Lett.*, 530, L93
- Temmink, K. D., Pols, O. R., Justham, S., Istrate, A. G., & Toonen, S. 2023, *Astronomy and Astrophysics*, 669, A45
- Thiele, S., Breivik, K., Sanderson, R. E., & Luger, R. 2023, *ApJ*, 945, 162
- Timpano, S. E., Rubbo, L. J., & Cornish, N. J. 2006, *Phys. Rev. D*, 73, 122001
- Tokovinin, A. 2014, *AJ*, 147, 87
- Tonry, J. L., Denneau, L., Heinze, A. N., et al. 2018, *PASP*, 130, 064505
- Toonen, S., Claeys, J. S. W., Mennekens, N., & Ruiter, A. J. 2014, *A&A*, 562, A14
- Toonen, S., Nelemans, G., & Portegies Zwart, S. 2012, *A&A*, 546, A70
- Toonen, S., Portegies Zwart, S., Hamers, A. S., & Bandopadhyay, D. 2020, *A&A*, 640, A16
- Tout, C. A., Pols, O. R., Eggleton, P. P., & Han, Z. 1996, *MNRAS*, 281, 257
- Triaud, A. H. M. J., Burgasser, A. J., Burdanov, A., et al. 2020, *Nature Astronomy*, 4, 650
- Valli, R., Graziani, L., & the LISA Synthetic UCB Catalogue Group. 2023, *arXiv e-prints*, arXiv:2311.03431
- van den Heuvel, E. P. J. 1976, in *IAU Symposium, Vol. 73, Structure and Evolution of Close Binary Systems*, ed. P. Eggleton, S. Mitton, & J. Whelan, 35
- van der Walt, S., Colbert, S. C., & Varoquaux, G. 2011, *Computing in Science and Engineering*, 13, 22
- van Zeist, W. G. J., Nelemans, G., Zwart, S. F. P., & Eldridge, J. J. 2024, *Astronomy and Astrophysics*, 691, A316
- von Zeipel, H. V. 1909, *Astronomische Nachrichten*, 183, 345
- Vynatheya, P., Hamers, A. S., Mardling, R. A., & Bellinger, E. P. 2022, *MNRAS*, 516, 4146
- Wilhelm, M. J. C., Korol, V., Rossi, E. M., & D'Onghia, E. 2021, *MNRAS*, 500, 4958
- Woods, T. E., Ivanova, N., van der Sluis, M. V., & Chaichenets, S. 2011, *The Astrophysical Journal*, 744, 12
- Xuan, Z., Naoz, S., Kocsis, B., & Michaely, E. 2024, *ApJ*, 965, 148
- Yu, S. & Jeffery, C. S. 2010, *A&A*, 521, A85
- Zhao, G., Zhao, Y., Chu, Y., Jing, Y., & Deng, L. 2012, *arXiv e-prints*, arXiv:1206.3569